Bioorganic Chemistry 92 (2019) 103189

Contents lists available at ScienceDirect

Bioorganic Chemistry

journal homepage: www.elsevier.com/locate/bioorg

Dual VEGFR-2/PIM-1 kinase inhibition towards surmounting the resistance to antiangiogenic agents *via* hybrid pyridine and thienopyridine-based scaffolds: Design, synthesis and biological evaluation

Ola H. Rizk[a,b], Mohamed Teleb[a], Marwa M. Abu-Serie[c], Omaima G. Shaaban[a,b,*]

[a] Department of Pharmaceutical Chemistry, Faculty of Pharmacy, Alexandria University, Alexandria 21521, Egypt
[b] Department of Pharmaceutical Chemistry, Faculty of Pharmacy & Drug Manufacturing, Pharos University in Alexandria, Alexandria, Egypt
[c] Medical Biotechnology Department, Genetic Engineering and Biotechnology Research Institute, City of Scientific Research and Technological Applications (SRTA-City), Egypt

ARTICLE INFO

Keywords:
Pyridine
Thienopyridine
Anticancer
Apoptosis
PIM-1 Kinase
VEGFR-2

ABSTRACT

Angiogenesis is a hallmark in cancer. Most antiangiogenic agents block the action of vascular endothelial growth factor (VEGF). In clinic, patients develop hypoxia-mediated resistance consistent with vascular responses to these agents. Recent studies underlying such resistance revealed hypoxia-inducible PIM-1 kinase upregulation which promotes cancer progression. PIM-1 kinase expression is thus viewed as a new resistance mechanism to antiangiogenic agents. Hence, combining PIM kinase inhibitors with anti-VEGF therapies provides synergistic antitumor response. Inspired by these facts, the current study aims at designing novel dual VEGFR-2/PIM-1 kinase inhibitors *via* molecular hybridization and repositioning of their pharmacophoric features. Moreover, enhancing the cytotoxic potential of the designed compounds was considered *via* incorporating moieties mimicking caspase 3/7 activators. Accordingly, series of novel pyridine and thieno[2,3-*b*]pyridine derivatives were synthesized and screened *via* MTT assay for cytotoxic activities against normal fibroblasts and four cancer cell lines (HepG-2, Caco-2, MCF-7 and PC-3). Compounds **3a, 9e**, **10b** and **10c** exhibited anticancer activities at nanomolar IC_{50} with promising safety, activated caspase 3/7 and induced apoptosis as well as DNA fragmentation more than doxorubicin in the four cancer cell lines. Furthermore, they exerted promising dual VEGFR-2/PIM-1 kinase inhibition and significantly exhibited higher therapeutic potential to alter the expression levels of VEGF, p53 and cyclin D than doxorubicin. Interestingly, the most active anticancer compound **10b** conferred the highest dual VEGFR-2/PIM-1 kinase inhibition. Finally, their *in silico* ligand efficiency metrics were acceptable.

1. Introduction

Cancer is considered the second most common cause of death worldwide [1]. The estimated new cancer cases increased from 14.1 millions in 2012 to 21.6 millions by 2030 [2]. In recognition of the burden posed by cancer, the WHO passed the resolution "*Cancer Prevention and Control through an Integrated Approach*" in 2017 [3]. Extensive studies have been conducted for identifying various cancer mechanisms [4], especially those underlying resistance to chemotherapy [5]. Within this context, the growth of new vascular network known as angiogenesis is viewed as a hallmark in cancer proliferation, as well as metastatic spread. One of the most essential regulators of angiogenesis is the vascular endothelial growth factor family (VEGFs). They exert their biological effects *via* targeting three correlated receptors (VEGFR 1-3) through interaction with their kinase domains [6]. VEGFR-2 represents the principle transducer of VEGF-dependent angiogenesis [7]. Therefore, inhibition of VEGF/VEGFR signaling pathway was recently reported as an advanced therapeutic target for inhibition of angiogenesis [8]. This inhibition is mainly achieved *via* preventing VEGFR-2 receptors activation utilizing receptor tyrosine kinase inhibitors (RTKIs) [9]. The most known inhibitors among the class are sunitinib [10], sorafenib [11], apatinib [12] and axitinib [13] (Fig. 1). Moreover, inhibition of VEGFR-2 can exert direct antiproliferative effect against cancer cell lines which express VEGFR-2 receptors on their surface. They induce apoptosis of these cells *in vitro* *via* blocking the VEGFR-2 downstream signaling pathways, as PI3K/AKT, and Ras-MEK-ERK pathways [14,15].

Although many antiangiogenic agents are currently approved for cancer treatment, patients usually develop rapid resistance to these drugs. This is attributed to reduced perfusion (hypoxia); the most

* Corresponding author.
E-mail address: omaima.shaaban@pua.edu.eg (O.G. Shaaban).

https://doi.org/10.1016/j.bioorg.2019.103189
Received 20 June 2019; Received in revised form 2 August 2019; Accepted 7 August 2019
Available online 08 August 2019
0045-2068/

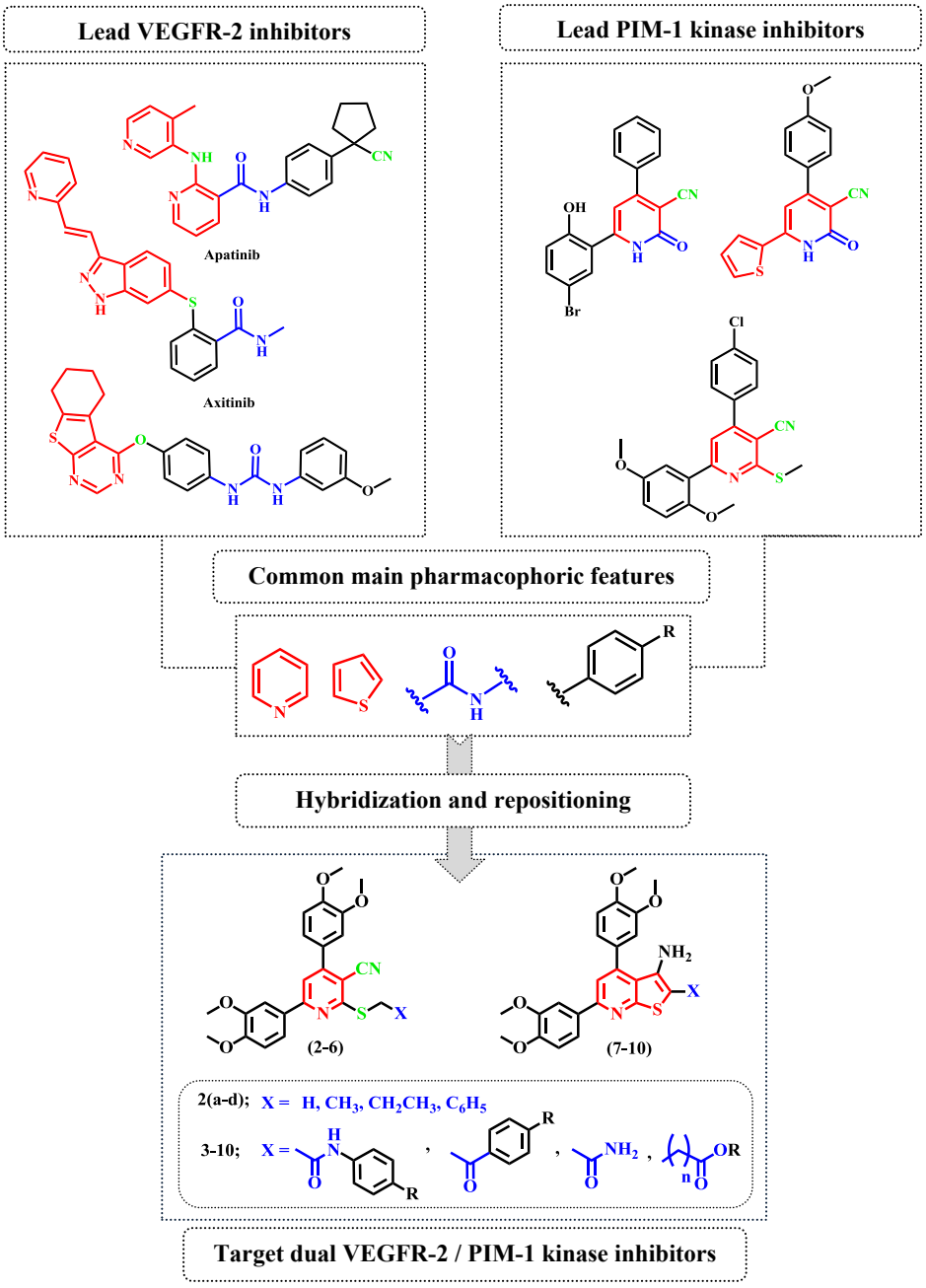

Fig. 1. Rationale for designing the target compounds.

common vascular response to antiangiogenic drugs. Consistent with hypoxia, several studies reported a measurable increase in hypoxia inducible factor-1 (HIF1) expression, which in turn induces the transcription of genes that promote various tumorigenesis processes, including angiogenesis [16,17]. Thus prolonged HIF1 activation is associated with the therapeutic resistance to antiangiogenic drugs [18]. New insights on the molecular mechanisms of tumor angiogenesis revealed that hypoxia-inducible PIM kinase upregulation also promotes such resistance [19]. It is worth mentioning that PIM-1 kinase, one of the serine/threonine kinases family, is basically involved in altering the transcription of key genes mediating tumorigenesis and angiogenesis such as; p53, cyclin D and VEGF [20–22]. Further studies focusing on the role of PIM kinase in mediating angiogenesis showed that PIM inhibition reduces HIF1 activity associated with hypoxia [19]. It comes as no surprise then that PIM inhibitors in combination with antiangiogenic drugs negates the tumor intrinsic defence mechanism. Moreover, antiangiogenic drugs starve cancer cells of oxygen, making them more hypoxic, thus more sensitive to PIM inhibitors. Accordingly, concomitant inhibition of VEGF and PIM achieves synergistic anticancer response that is characterized by growth arrest, decreased angiogenesis, enhanced cell death, and reduced metastasis [19]. Besides that, effective cancer treatment strategies usually encompass apoptotic induction which is mainly accomplished *via* caspase 3/7 activation [23,24].

Structure activity relationship studies showed that potent VEGFR-2 inhibitors share certain structural features that are thematic across most of the class members comprising a flat heterocyclic aromatic ring constructing the core, a hydrogen bond acceptor-donor pair, which is either an amide or urea moiety, and a terminal aromatic ring with a space sufficient enough for various substituents around it [6,25]. On the other hand, most of the potent PIM-1 kinase inhibitors share a characteristic cyanopyridine core that is usually substituted with different aryl moieties at positions 4 and 6 [26,27]. Interestingly, pyridine

constructs a pharmacophoric core of some lead caspase 3/7 activators [28] Moreover, literature survey revealed that pyridine ring is extensively present in the skeletal backbone of many lead anticancer agents [29,30] and VEGFR-2 inhibitors [31] including commercially available drugs as apatinib and axitinib (Fig. 1).

With the aforementioned advantages of combining inhibition of VEGFR-2 and PIM-1 kinases together with caspase 3/7 activation, the current study aims at designing novel dual VEGFR-2/PIM-1 kinase inhibitors endowed with caspase 3/7 activation potential. The design strategy was rationalized *via* applying molecular hybridization and repositioning of the common respective pharmacophoric features (Fig. 1). Within this approach, pyridine moiety was selected as the heterocyclic core endowed with an amide moiety representing the hydrogen bond acceptor-donor motif linked to a terminal aromatic ring. This VEGFR-2 inhibitor inspired scaffold was then decorated with a cyano moiety and two aryl (3,4-dimethoxyphenyl) groups at positions 3, 4 and 6, respectively to mimic the PIM kinase inhibitors' general structural features. It is worth mentioning that the aryl groups were selected as dimethoxyphenyl groups which were reported to enhance the anticancer activity through improving compounds' lipophilicity [29,30]. To enrich the structure-activity relationship study, the designed scaffold was modified at various positions, where the pyridine heterocyclic core was replaced with thienopyridine ring, the amide moiety was replaced with carboxylate, ketonic, or alkyl groups, finally the terminal aromatic ring was substituted with various moieties. All the newly synthesized compounds were screened for cytotoxic activities against normal human fibroblasts and four human cancer cell lines; HepG-2 (liver), Caco-2 (colon), MCF-7 (breast), PC-3 (prostate) utilizing MTT assay [32]. Their respective selectivity indices were calculated to assess their efficacy and safety profiles. The most active compounds were evaluated for their ability to *in vitro* inhibit VEGFR-2 and PIM-1 kinase enzymes, then subjected to real time PCR assay for quantifying VEGF, p53 and cyclin D expression levels. Furthermore, the most promising anticancer compounds were tested for their potential to induce apoptosis by flow cytometric annexin V/propidium iodide analysis, caspase 3/7 activation assay and subsequent DNA fragmentation. Finally, ligand efficiency metrics of the most active compounds were computationally predicted as a useful tool for selecting and optimizing lead compounds.

2. Results and discussion

2.1. Chemistry

Several multi-component reaction (MCR) strategies have been reported to efficiently prepare cyanopyridines [30,33]. In this study, the synthetic strategies adopted for the synthesis of the intermediate and target compounds are depicted in Schemes 1 And 2. Scheme 1 outlined the preparation of pyridine-2-thione **1** through one pot reaction of dimethoxyacetophenone with dimethoxybenzaldehyde and cyanothioacetamide in the presence of catalytic amount of ammonium acetate. The infrared spectrum showed a characteristic absorption bands at 3444 and 2216 cm^{-1} corresponding to NH and CN groups, respectively ^1H NMR showed a singlet at δ 3.88 ppm corresponding to the $4OCH_3$ moieties. S-alkylation of **1** with alkyl halides, ethyl bromoacetate and ethyl bromopropionate in the presence of potassium carbonate by refluxing in absolute ethanol yielded compounds **2a-d** and **3a, b**, respectively following the reported reaction conditions [34]. IR spectra of **2a-d** and **3a, b** lacked the high frequency NH stretching absorption bands and showed absorption bands at 1729 and 1742 cm^{-1} corresponding to C═O groups of compound **3a, b.** S-alkylation with α-bromoketones could be performed under different conditions [35]. Herein, Reaction of **1** with 4-substituted phenacyl bromides or *N*-aryl-2-chloroacetamides in the presence of anhydrous sodium acetate in absolute ethanol at room temperature afforded the corresponding oxoethylthio derivatives **4a-d** or *N*-aryl thioacetamides **5a-e**, respectively. The molecular structures of these compounds were confirmed on the basis of their spectral data. The infrared spectra for compounds **4a-d** showed characteristic bands at 1691–1702 cm^{-1} corresponding to C═O groups. The ^1H NMR spectra showed additional singlets for methylene group of SCH_2 at δ 5.08–5.14 ppm as well as signals assigned for the aryl groups at their expected chemical shifts. For compounds **5a-e**, their infrared spectra displayed absorption bands at 3259–3290 cm^{-1} and 1662–1668 cm^{-1}corresponding to the amide moieties. Additionally their ^1H NMR spectra displayed two D_2O exchangeable singlets at δ 10.21–10.51 and 13.93–13.94 ppm corresponding to the NH protons. Interestingly, S-alkylation of **1** with chloroacetonitrile following the same reaction conditions used for preparation of compounds **2a-d** and **3a, b** afforded compound **6** where S-alkylation is followed by alkaline hydrolysis of the cyano group to the corresponding thioacetamide derivative [36]. IR spectrum of **6** revealed absorption bands at 3467, 3335 cm^{-1} and 1632 cm^{-1}corresponding to the amide moiety, and its ^1H NMR spectrum showed a singlet of the SCH_2 at δ 4.43 ppm and D_2O exchangeable singlet at δ 5.76 ppm corresponding to the NH_2 protons.

In scheme 2, Cyclization of the S-alkylated pyridine derivatives **3a** and **6** by refluxing in freshly prepared sodium ethoxide solution afforded the thieno[2,3-*b*]pyridine-2-carboxylic acid salt **7** and the thieno [2,3-*b*]pyridine-2-carboxamide **8**, respectively [37]. IR spectrum of **7** lacked the cyano absorption band in **3a** and revealed amino absorption bands at 3415 and 3330 cm^{-1}. Furthermore, ^1H NMR spectrum lacked the triplet and quartet of the ethyl ester moiety, and the singlet of the SCH_2 in the precursor **3a.** IR spectrum of **8** lacked the cyano absorption band and its ^1H NMR spectrum lacked the singlet of the SCH_2 in the precursor **6.**

The thienopyridines **9a-e** and **10a-e** were prepared by refluxing pyridine-2-thione **1** with appropriate phenacyl bromide or chloroacetanilide derivatives, in presence of anhydrous potassium carbonate in absolute ethanol. IR spectra of **9a-e** and **10a-e** lacked the cyano absorption band in **1** and revealed amino absorption bands in the range of 3467–3485 and 3290–3362 cm^{-1}.The structure of such compounds were additionally substantiated on basis of their ^1H NMR and ^{13}C NMR spectral data.

2.2. Biological evaluation

2.2.1. Cytotoxicity screening

All the newly synthesized compounds were evaluated for their cytotoxic effects against normal human lung fibroblasts (Wi-38) using doxorubicin (Dox) as standard anticancer drug utilizing microculture MTT method [32,38,39]. The highest IC_{50} values indicate that the compounds were safe on the proliferation of normal human cells. As shown in Table 1, all prepared compounds possessed a remarkable non cytotoxic effect on human lung fibroblasts (Wi-38) with IC_{50} ranging from 0.0289 to 0.7790 μM compared to doxorubicin (IC_{50} = 0.0266 μM). Compounds **1, 2b**, **3b**, **5d**, **10a** and **10d** showed the highest IC_{50} values > 0.0927 μM which indicate their safety on normal human cells.

2.2.2. Anticancer screening

All the new compounds were screened for their potential anticancer activities against four human cancer cell lines; HepG-2 (liver), Caco-2 (colon), MCF-7 (breast), PC-3 (prostate) using doxorubicin (Dox) as standard anticancer drug utilizing microculture MTT assay, as described by Mosmann [32]. The obtained data were represented in Table 1 as IC_{50} values of the tested compounds and the reference drug doxorubicin in μM. The results revealed that some compounds showed significant anticancer activities against all tested cell lines. The most potent activities against HepG-2 cell line were exhibited by compounds **10b** and **10c** with IC_{50} values = 0.0062 and 0.0090 μM, respectively compared to doxorubicin (IC_{50} = 0.0100 μM). While compounds **3a** and **9e** showed nearly equipotent activities with IC_{50} values = 0.0123 and 0.0130 μM, respectively. The results demonstrate that Caco-2 cell line was sensitive to all the tested compounds except **1, 2a, 2c, 4a** and **10e** with IC_{50} values in the range of 0.0594–0.0952 μM compared to

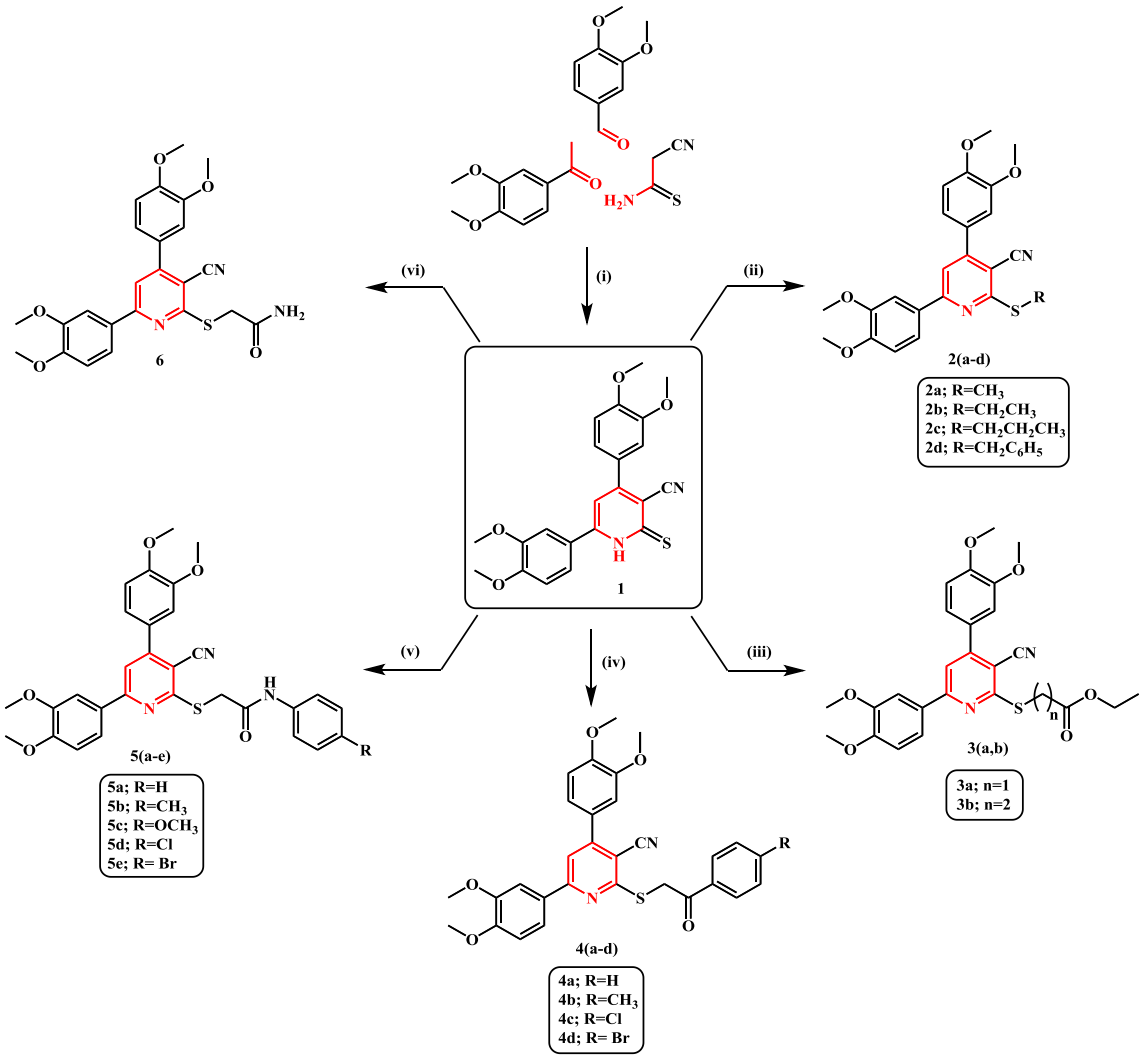

Reagents and conditions : (i) CH_3COONH_4 / EtOH / Reflux ; (ii) Alkyl halide / K_2CO_3 / EtOH / Reflux; (iii) $Br(CH_2)_nCOOEt$ /K_2CO_3 / EtOH / Reflux; (iv) *p*-$RC_6H_4COCH_2Br$ / CH_3COONa / EtOH / R.T. ; (v) *p*-$RC_6H_4NHCOCH_2Cl$ / CH_3COONa / EtOH / R.T. ; (vi) $ClCH_2CN$ / K_2CO_3 / EtOH / Reflux.

Scheme 1. Synthetic pathway for pyridine derivatives 1–6.

doxorubicin (IC_{50} = 0.0504 μM). Compounds **3a, 9b, 9e, 10b, 10c** and **10d** showed the highest potency against Caco-2 cell line (more than doxorubicin) with IC_{50} values ranging from 0.0103 to 0.0249 μM. The antitumor activity of the tested compounds against MCF-7 cell line revealed that four compounds **3a, 9e, 10b** and **10c** (IC_{50} = 0.0179, 0.0163, 0.0127 and 0.0169 μM, respectively) exhibited superior activities than doxorubicin (IC_{50} = 0.0234 μM), while compounds **2a**, **2c** and **10d** were nearly equipotent to doxorubicin with IC_{50} values ranging from 0.0250 to 0.0299 μM. Regarding the anticancer activity against the PC-3 cell line, compounds **3a, 9e, 10b** and **10c** (IC_{50} = 0.0209, 0.0161, 0.0105 and 0.0202 μM, respectively) were more potent than doxorubicin (IC_{50} = 0.0332 μM), whereas compounds **5e** and **6** showed promising activity with IC_{50} values 0.0361 and 0.0327 μM, respectively. Accordingly, compounds **3a, 9e, 10b** and **10c** exhibited the highest anticancer potential, against all tested human cancer cells, compared to other compounds and doxorubicin.

Selectivity index is the ratio between the compound IC_{50} on normal cells and its IC_{50} on cancer cells (Table 1), which is the measure of the selectivity of the drug candidate towards cancer cells rather than normal cells. When the SI is ≥3, the drug is considered to be highly selective [40]. It is one of the most important measure of an anticancer agent that shows its ability to differentiate between normal and cancer cells [41].

Accordingly, the tested compounds were evaluated for their selectivity index values (SI). Hence, compounds **3a, 9e, 10b** and **10c** were found to be promising anticancer agents especially against liver cancer (HepG-2) with SI values 4.772, 3.038, 9.516 and 5.900, respectively. Moreover, compounds **3a** and **10b** were selective against colon cancer cell line (Caco-2) with SI; 5.699 and 2.864, respectively. Additionally, compounds **3a** and **10c** showed high SI of 3.262 and 3.142, respectively against MCF-7 breast cancer cell lines and moderate SI of 2.808 and 2.628, respectively towards prostate cancer (PC-3). Compound **9e** showed moderate SI toward MCF-7 and PC3 cell lines. Both compounds (**3a** and **10c**) showed the highest cancer SIs towards all tested cancer cell lines in comparison with Dox, while compound **9e** had the highest SIs against HepG-2, MCF-7 and PC-3 cell lines. Finally, compound **10b** revealed high selectivity against HepG-2 and Caco-2 cell lines compared to Dox. It is worth mentioning that compounds **2b** and **10a** were found to have high SIs towards all cancer cell lines although they lack anticancer activities this is because of their higher IC_{50} Values (0.7790 and 0.2130 μM, respectively) on wi-38 normal cell than IC_{50} values on cancer cells.

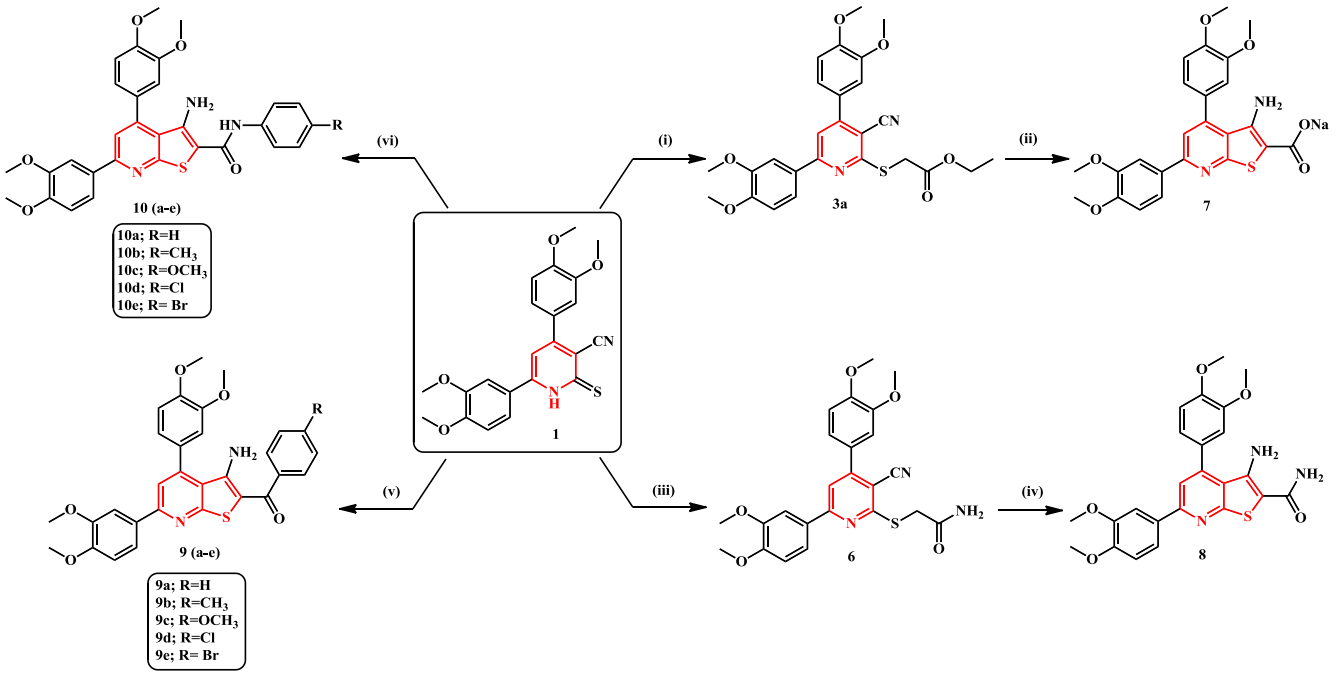

Reagents and conditions : (i) $BrCH_2COOEt$ / K_2CO_3/ EtOH/ Reflux ; (ii) C_2H_5ONa / EtOH / Reflux ; (iii) $ClCH_2CN$ / K_2CO_3 / EtOH / Reflux; (iv) C_2H_5ONa / EtOH / Reflux ; (v) *p*-$RC_6H_4COCH_2Br$ / K_2CO_3 / EtOH / Reflux; (vi) *p*-$RC_6H_4NHCOCH_2Cl$ / K_2CO_3 / EtOH / Reflux.

Scheme 2. Synthetic pathway for thienopyridine derivatives 7–10.

Table 1
In vitro cytotoxicity and selectivity index (SI) values of the tested compounds.

Cpd No.	wi-38		HepG-2		Caco-2		MCF-7		PC-3	
	IC_{50} (μM)	EC_{100} (μM)	IC_{50} (μM)	SI	IC_{50} (μM)	SI	IC_{50} (μM)	SI	IC_{50} (μM)	SI
1	0.0927 ± 0.006	0.0416 ± 0.015	0.0924 ± 0.004	1.003	0.0843 ± 0.01	1.099	0.1238 ± 0.028	0.748	0.1180 ± 0.02	0.785
2a	0.0625 ± 0.004	0.0240 ± 0.018	0.0347 ± 0.002	1.801	0.0594 ± 0.01	1.052	0.0299 ± 0.003	2.090	0.0470 ± 0.006	1.329
2b	0.7790 ± 0.006	0.0480 ± 0.02	0.0486 ± 0.002	16.028	0.0390 ± 0.001	19.964	0.0476 ± 0.001	16.365	0.0553 ± 0.01	14.086
2c	0.0514 ± 0.003	0.0169 ± 0.006	0.0960 ± 0.014	0.535	0.0837 ± 0.002	0.614	0.0254 ± 0.0005	2.023	0.0800 ± 0.0002	0.642
2d	0.0549 ± 0.004	0.0326 ± 0.007	0.0525 ± 0.007	1.045	0.0375 ± 0.0003	1.464	0.0438 ± 0.002	1.253	0.0461 ± 0.001	1.193
3a	0.0587 ± 0.014	0.0473 ± 0.03	0.0123 ± 0.004	4.772	0.0103 ± 0.0002	5.699	0.0179 ± 0.001	3.262	0.0209 ± 0.001	2.808
3b	0.0998 ± 0.045	0.0617 ± 0.026	0.0466 ± 0.005	2.141	0.0391 ± 0.003	2.552	0.0414 ± 0.004	2.410	0.0476 ± 0.005	2.096
4a	0.0615 ± 0.013	0.0408 ± 0.013	0.0898 ± 0.02	0.684	0.0952 ± 0.003	0.646	0.0748 ± 0.02	0.822	0.0592 ± 0.003	1.038
4b	0.0340 ± 0.002	0.0083 ± 0.001	0.0635 ± 0.01	0.535	0.0432 ± 0.001	0.787	0.0416 ± 0.0004	0.817	0.0441 ± 0.0001	0.770
4c	0.0553 ± 0.035	0.0215 ± 0.019	0.0712 ± 0.002	0.776	0.0528 ± 0.0005	1.047	0.0610 ± 0.0001	0.906	0.0648 ± 0.0006	0.853
4d	0.0361 ± 0.0003	0.0250 ± 0.001	0.0644 ± 0.001	0.560	0.0512 ± 0.001	0.705	0.0540 ± 0.003	0.668	0.0691 ± 0.009	0.522
5a	0.0299 ± 0.002	0.0105 ± 0.01	0.0723 ± 0.003	0.413	0.0540 ± 0.005	0.553	0.0489 ± 0.0008	0.611	0.0510 ± 0.001	0.586
5b	0.0333 ± 0.001	0.0157 ± 0.004	0.0451 ± 0.001	0.738	0.0366 ± 0.006	0.909	0.0390 ± 0.001	0.853	0.0540 ± 0.002	0.616
5c	0.0370 ± 0.003	0.0268 ± 0.006	0.0581 ± 0.005	0.637	0.0373 ± 0.001	0.991	0.0418 ± 0.003	0.885	0.0468 ± 0.001	0.790
5d	0.1190 ± 0.07	0.0639 ± 0.03	0.0413 ± 0.001	2.881	0.0294 ± 0.007	4.047	0.0360 ± 0.002	3.305	0.0586 ± 0.01	2.030
5e	0.0700 ± 0.031	0.0350 ± 0.02	0.045 ± 0.003	1.555	0.0317 ± 0.002	2.209	0.0383 ± 0.003	1.828	0.0361 ± 0.002	1.940
6	0.0415 ± 0.003	0.0166 ± 0.016	0.042 ± 0.001	0.988	0.0317 ± 0.004	1.309	0.0325 ± 0.003	1.276	0.0327 ± 0.0001	1.269
7	0.0770 ± 0.014	0.0630 ± 0.01	0.0751 ± 0.001	1.025	0.0545 ± 0.002	1.412	0.0728 ± 0.018	1.057	0.0720 ± 0.008	1.069
8	0.0510 ± 0.002	0.0421 ± 0.003	0.0619 ± 0.002	0.823	0.0282 ± 0.006	1.808	0.0347 ± 0.004	1.469	0.0484 ± 0.002	1.053
9a	0.0289 ± 0.006	0.0111 ± 0.001	0.0614 ± 0.001	0.470	0.0495 ± 0.002	0.583	0.0495 ± 0.003	0.583	0.0504 ± 0.001	0.573
9b	0.0399 ± 0.001	0.0301 ± 0.001	0.0426 ± 0.0003	0.936	0.0249 ± 0.001	1.602	0.0362 ± 0.001	1.102	0.0950 ± 0.001	0.420
9c	0.0383 ± 0.005	0.0193 ± 0.007	0.0734 ± 0.002	0.521	0.0544 ± 0.004	0.704	0.0571 ± 0.004	0.670	0.0815 ± 0.02	0.426
9d	0.0307 ± 0.012	0.0287 ± 0.006	0.0476 ± 0.001	0.644	0.0381 ± 0.0005	0.805	0.0529 ± 0.012	0.580	0.0463 ± 0.005	0.663
9e	0.0395 ± 0.001	0.0317 ± 0.003	0.0130 ± 0.001	3.038	0.0237 ± 0.001	1.666	0.0163 ± 0.004	2.423	0.0161 ± 0.004	2.453
10a	0.2130 ± 0.04	0.0194 ± 0.004	0.0446 ± 0.002	4.775	0.0366 ± 0.001	5.819	0.0389 ± 0.003	5.475	0.0427 ± 0.0005	4.988
10b	0.0590 ± 0.018	0.0472 ± 0.014	0.0062 ± 0.001	9.516	0.0206 ± 0.002	2.864	0.0127 ± 0.025	0.574	0.0105 ± 0.0193	0.533
10c	0.0531 ± 0.005	0.0312 ± 0.01	0.0090 ± 0.001	5.900	0.0239 ± 0.002	2.221	0.0169 ± 0.0003	3.142	0.0202 ± 0.002	2.628
10d	0.0927 ± 0.034	0.0764 ± 0.027	0.0464 ± 0.003	1.997	0.0245 ± 0.001	3.783	0.0253 ± 0.0001	3.664	0.0503 ± 0.008	1.842
10e	0.0363 ± 0.002	0.0294 ± 0.003	0.0722 ± 0.005	0.503	0.0615 ± 0.001	0.590	0.0735 ± 0.004	0.494	0.0735 ± 0.007	0.489
Dox	0.0266 ± 0.005	0.0121 ± 0.001	0.0100 ± 0.001	2.660	0.0504 ± 0.005	0.527	0.0234 ± 0.002	1.136	0.0332 ± 0.001	0.801

Data were expressed as the means of two determinations ± SEM.

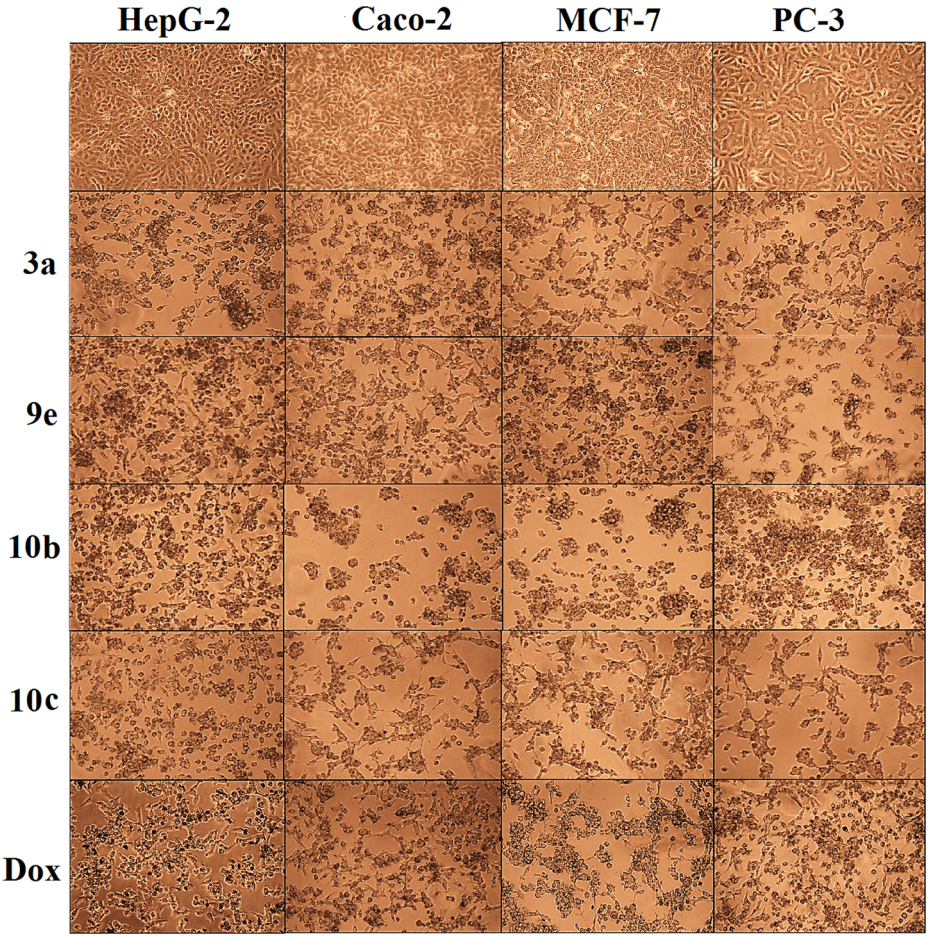

Fig. 2. Morphological alterations of the most effective compounds-treated cancer cell lines, untreated cancer cells and doxorubicin-treated cells.

Furthermore, the four cancer cell lines (HepG-2, Caco-2, MCF-7 and PC-3) were examined for morphological changes before and after treatment with the most active and safe compounds **3a, 9e, 10b** and **10c** in comparison with cells treated with the reference doxorubicin. As revealed, these compounds were able to collapse normal spindle shape of four studied cancer cell lines as shown in Fig. 2.

2.2.3. Flow cytometric analysis of apoptosis

Compounds **3a, 9e, 10b** and **10c** exhibiting significant anticancer activities were tested for their apoptotic effects using flow cytometric annexin V/propidium iodide analysis [42]. Results **(**Fig. 3 and Table 2**)** revealed high percentages of annexin-stained population cells in cancer cell lines treated with compounds **3a, 9e, 10b** and **10c** compared to the control untreated cancer cells. It was obvious that these compounds induced apoptosis-dependent death by above 40% in the treated HepG-2, Caco-2, MCF-7 and PC-3 cancer cell lines compared to less than 39% apoptotic cell in case of Dox. Compound **10b** exhibited the highest significant potential for induction of apoptosis (> 64%, early apoptosis; 15.35–39.77% and late apoptosis; 31.37–55.53%) in all studied human cancer cell lines. Compound **9e** was able to induce apoptosis by approximately similar percentages at early and late stages in HepG-2 and Caco-2 cells, whereas higher percentages were detected at late stages in case of MCF-7 and PC-3. **3a** majorly induced late apoptosis in Caco-2, PC-3 and HepG-2, whereas it mainly induced early apoptosis in MCf-7. No significant differences were observed between early and late apoptotic populations in all the screened cell lines treated with **10c.**

2.2.4. Caspase 3/7 activation assay and the subsequent DNA fragmentation

Caspase 3/7 activators are well known as apoptotic inducers [43,44]. Herein, the apoptotic induction mechanism displayed by the most active compounds **3a, 9e, 10b** and **10c** was estimated by determining the percentages of caspase 3/7 activation in cancerous cell lines when treated with IC_{50} of these compounds. Results (Table 3**)** revealed that all compounds **3a, 9e, 10b** and **10c** significantly induced caspase 3/7 activation (> 45%) higher than the reference; Dox (42.94–48.09%) in all tested human cancer cell lines. Compound **10b** exhibited the highest significant caspase activation (56.86–62.85%) in all four tested human cancer cells in comparison with other compounds and Dox. Consequently, DNA fragmentation induced in all cancer cell lines exposed to the four active compounds (> 49%) were higher than that in Dox-treated cancer cells (< 45.9%). Compound **10b** exhibited the highest DNA fragmentation potential (> 77.5%) among the tested compounds and Dox in all studied human cancer cells (Table 4). Accordingly, results of the caspase 3/7 activation assay and the subsequent DNA damage were consistent with that of the flow cytometric analysis of apoptosis.

2.2.5. VEGFR-2 kinase inhibitory activity

Based on the aforementioned role of VEGFR-2 inhibition as promising therapeutic strategy for inhibiting angiogenesis and tumor growth, the most active anticancer compounds **(3a, 9e, 10b** and **10c)** were evaluated for their VEGFR-2 kinase inhibitory activity [45] compared to quercetin as reference. Their IC_{50} values were listed in Table 5. Results revealed promising VEGFR-2 kinase inhibition with IC_{50} values ranging from 5.873 to 12.411 μM. Remarkably, compounds **10b** (IC_{50} = 5.873 μM) and **9e** (IC_{50} = 6.905 μM) exhibited inhibitory activities comparable to quercetin (IC_{50} = 5.219 μM), whereas **10c** and **3a** were less active.

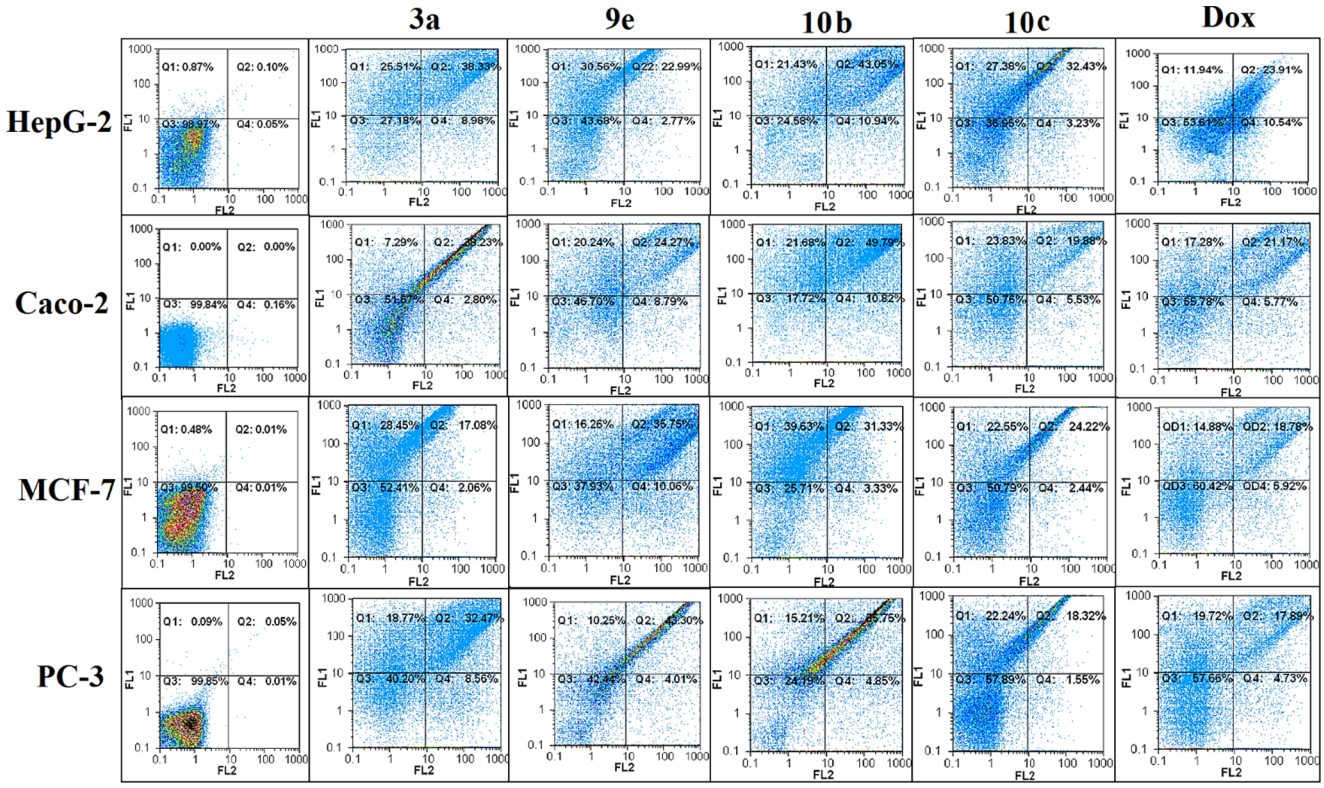

Fig. 3. Flow charts of annexin-PI analysis of the most effective compounds-treated cancer cells lines, untreated cancer cells and doxorubicin-treated cells.

2.2.6. PIM-1 kinase inhibitory activity

In search for novel dual VEGFR-2/PIM-1 kinase inhibitors towards achieving synergistic anticancer response, PIM-1 kinase inhibitory activity [46] was evaluated for the most active compounds **(3a, 9e, 10b** and **10c)** and the IC_{50} values were recorded in Table 5. Quercetin, was used as the reference drug. The results revealed remarkable PIM-1 kinase inhibitory activities with IC_{50} values ranging from 7.948 to 12.163 µM comparable to the reference drug (IC_{50} = 11.436 µM). Interestingly, among them, compounds **3a, 9e** and **10b** showed superior inhibitory activities to quercetin with IC_{50} = 9.236, 9.394 and 7.948 µM, respectively. Moreover, compound **10c** was comparable to quercetin with IC_{50} = 12.163 µM.

2.2.7. Real time PCR assay for quantifying VEGF, p53 and cyclin D expression levels

Compounds **3a, 9e, 10b** and **10c** were then subjected to real time PCR assays [47] for quantifying their effect on expression levels of some key player genes (VEGF, p53 and cyclin D) underlying angiogenesis and carcinogenesis. Results in Table 6 indicated that both compounds **3a** and **10b** suppressed the expression of VEGF and cyclin D by 4 and 5 folds, respectively, in the treated HepG-2 cells, while **9e** and **10c** exhibited lower potential to decrease the expression levels of the above-mentioned genes by approximately 3 and 4 folds, respectively. Moreover, compounds **3a** and **10b** upregulated p53 expression by 3 folds, whereas **9e** and **10c** induced 2-fold upregulation. Interestingly, all the tested compounds significantly exhibited higher therapeutic potential to alter the expression levels of VEGF, p53 and cyclin D than the reference chemotherapy; doxorubicin.

2.2.8. Structure activity relationship

In the light of the MTT results, the general activity pattern showed that the designed scaffolds conserved the intrinsic antitumor effects of the parent lead compounds (Fig. 1). However, the displayed activity and selectivity appeared to be a function of the scaffold building blocks. Seemingly, the majority of the most potent compounds belong to the thienopyridine series, with the *p*-tolyl acetamido derivative **10b** at the top of the list. In other words, the combination of thienopyridine core, amide linker and *p*-tolyl as a terminal aromatic moiety conferred the highest anticancer activity against the four screened cell lines with nanomolar IC_{50} values. Within this series, the terminal aromatic ring substitution endowed variable anticancer activities. Oxygen insertion (*p*-methoxy derivative **10c**) slightly decreased the anticancer activity against all the screened cancer cell lines. Replacing the *p*-methyl moiety **(10b)** with chloro **(10d)** obviously decreased the anticancer potency against HepG-2, MCF-7 and PC-3, while maintaining approximately similar activity against Caco-2 cells. Such selectivity against Caco-2 was partially lost in case of the unsubstituted derivative **(10a),** which showed general lower anticancer activity than both **10b** and **10c**. The *p*-bromo derivative **(10e)** exhibited the lowest activities among the series. Further comparison of the anticancer activities within the thienopyridine-based derivatives revealed that replacement of the amide linker with carbonyl moiety (i.e. NH removal; compounds **9a-e**) generally led to lower potencies. Surprisingly, within this series, the aromatic substitution pattern contributed differently to the observed activity, where the *p*-bromo derivative **(9e)** exhibited the highest activities against the four cell lines. The *p*-methyl derivative **(9b)** endowed approximately similar activity against Caco-2 cells, lower potency against HepG-2 and MCF-7, and abolished activity against PC-3. Interestingly, replacement of the methyl group with hydrogen (unsubstituted derivative; **9a**) or chloro **(9d)** restored considerable anticancer activity against PC-3, while other cell lines were less sensitive to such modifications. On the other hand, oxygen insertion (*p*-methoxy derivative; **9c**) remarkably decreased the anticancer activity against all the screened cancer cell lines. More structure activity relationship studies were concluded with the terminal aromatic ring removal while keeping the amide linker **(8)** or replacing it with a carboxylate group **(7)**. Within this context, the unsubtituted amide linker **(8)** nearly conserved the intrinsic anticancer activity of the phenyl acetamido derivative **10a** against MCF-7 and PC-3. Moreover, it endowed higher potency against Caco-2 and lower one against HepG-2. In other words, the unsubstituted terminal aromatic

Table 2
Percentages of the apoptotic cell populations in the most active compounds-treated cancer cell lines.

Cpd No.	HepG-2			Caco-2			MCF-7			PC-3		
	Early apoptosis %	Late apoptosis %	Total Apoptosis %	Early apoptosis %	Late apoptosis %	Total apoptosis %	Early apoptosis %	Late apoptosis %	Total apoptosis %	Early apoptosis %	Late apoptosis %	Total apoptosis %
Untreated Cells	0.78 ± 0.09	0.1 ± 0.001	0.169 ± 0.02^{f}	0 ± 0	0.005 ± 0.005	0.05 ± 0.005^{d}	0.47 ± 0.01	0.01 ± 0.001	0.48 ± 0.01^{e}	0.06 ± 0.03	0.045 ± 0.005	0.105 ± 0.035^{f}
3a	25.01 ± 0.5	37.71 ± 0.62	**62.72 ± 1.12**^{bc}	7.22 ± 0.07	38.14 ± 0.085	**45.36 ± 0.155**^{b}	28.22 ± 0.22	16.99 ± 0.08	45.22 ± 0.31^{c}	18.46 ± 0.3	32.28 ± 0.19	50.74 ± 0.49^{c}
9e	29.81 ± 0.74	22 ± 0.99	51.81 ± 1.73^{d}	19.91 ± 0.32	23.97 ± 0.3	43.88 ± 0.625^{b}	16.2 ± 0.06	35.61 ± 0.14	**51.81 ± 0.2**^{b}	20.36 ± 1.02	33.11 ± 1.01	**53.48 ± 0.07**^{b}
10b	21.49 ± 0.06	43.08 ± 0.03	**64.57 ± 0.095**^{a}	21.95 ± 0.27	49.57 ± 0.21	**71.52 ± 0.05**^{a}	39.77 ± 0.14	31.73 ± 0.4	**71.5 ± 0.54**^{a}	15.35 ± 0.14	55.53 ± 0.22	**70.88 ± 0.07**^{a}
10c	26.99 ± 0.38	31.78 ± 0.65	58.77 ± 1.035^{b}	23.51 ± 0.32	19.48 ± 0.39	42.99 ± 0.715^{b}	22.32 ± 0.23	24.11 ± 0.11	46.43 ± 0.34^{c}	22.13 ± 0.11	18.15 ± 0.16	40.28 ± 0.27^{d}
Dox	11.99 ± 0.05	24.09 ± 0.18	36.08 ± 0.23^{e}	17.67 ± 0.39	21.59 ± 0.42	39.26 ± 0.81^{c}	15.04 ± 0.16	18.93 ± 0.15	33.97 ± 0.31^{d}	19.88 ± 0.16	18.01 ± 0.12	37.89 ± 0.28^{e}

All values are expressed as mean ± SEM.
Different letters are significantly different in the same column at $P < 0.05$.

ring conferred anticancer activity against HepG-2 cells. However, it wasn't essential structural feature for anticancer activities against Caco-2, MCF-7 and PC-3. Concerning the carboxylate derivative **7**, it is obvious that replacing the amide linker with unsubstituted carboxylate moiety decreased the anticancer activity towards all the screened cell lines. On the other hand, systematic investigation of the pyridine based derivatives **(1–6)** revealed that the most active compound incorporated a carboxylate linker capped with ethyl moiety **(3a)**. Positioning of the ethyl carboxylate moiety with respect to the pyridine core was critical, where the activity was optimized with 3-bonds distance **(3a).** Increasing that distance (4 bonds; **3b**) obviously decreased the anticancer potency against all the screened cell lines. Further structure activity relationship studies around the lead compound **3a** showed that removal of the carboxylate moiety while keeping different alkyl groups **(2a-c)** led to variable anticancer activities against the screened cell lines. In this series, methyl group **(2a)** endowed the highest potency against HepG-2 and PC-3. Increasing the alkyl group size to ethyl **(2b)** generally decreased the activity against all the screened cells except for Caco-2. Moreover, propyl group **(2c)** led to far lower anticancer activity towards all the tested cell lines while exceptionally conferring the highest activity against MCF-7 cells. Interestingly, capping the methyl group with terminal phenyl ring **(2d)** endowed the highest recorded potency against Caco-2 among the series. Carbonyl group insertion **(4a)** led to far lower potency**.** Further investigation of various substituents incorporated in the terminal phenyl ring revealed that the *p*-methyl moiety conferred the highest activity among the group. Results also showed that compounds incorporating an amide linked to the pyridine based scaffold **(5a-e, 6)** are generally more potent than those with carbonyl linker **(4a-e)**. Within this series, the unsubstitued amide derivative **6** was among the most active compounds especially against PC-3 cells, whereas the amide derivative with terminal *p*-chlorophenyl moiety **(5d)** exhibited the highest anticancer activity against HepG-2, MCF-7 and Caco-2 cells. Finally, removal of both the linker and terminal aromatic or aliphatic moieties **(1)** abolished the anticancer activity. This highlights the significance of the rationalized assembly of pharmacophoric features in the current study **(**Fig. 1**).**

Mechanistic studies showed that the assembly of thienopyridine core, amide linker and *p*-tolyl as a terminal aromatic moiety **(10b)** conferred the highest dual VEGFR-2/PIM-1 kinase inhibition, best VEGF expression suppression and caspase 3/7 activation which were consistent with the anticancer results. Terminal aromatic group modification *via* oxygen insertion (*p*-methoxy derivative **10c**) critically decreased the PIM kinase inhibitory activity, while maintaining moderate VEGFR-2 inhibition. *p*-Bromo substitution and amide replacement with carbonyl group **(9e)** maintained approximately the highest detected potency against VEGFR-2 with moderate PIM-1 kinase inhibition activity. On the other hand, replacing the thienopyridine core with pyridine, amide with ester and terminal aryl with ethyl group **(3a)** shifted the inhibitory activity towards PIM-kinase side. Although, such modification didn't allow potential VEGFR-2 inhibition, it conferred VEGF suppression comparable to the most active thienopyridine derivative **10b.**

2.2.9. In silico ligand efficiency metrics

Recent studies utilize ligand efficiency (LE) as a useful lead optimization tool. This parameter describes the balance between potency and molecular size, which is related to various pharmacokinetic and toxicological parameters [48–50]. LE measures the average binding energy per non-hydrogen atom instead of considering the binding affinity of the whole molecule, thus it allows comparing and prioritizing ligands corrected for their sizes. LE can be calculated from following equations [51]:

$$LE = \Delta G/NHA = 1.37(pIC_{50})/NHA$$

Where:

Table 3
Percentages of caspase 3/7 activation in the most active compounds-treated cancer cell lines.

Cpd No.	Caspase 3/7 activation %			
	HepG-2	Caco-2	MCF-7	PC-3
3a	52.59 ± 1.05^{b}	50.92 ± 0.405^{b}	45.96 ± 0.28^{c}	49.31 ± 0.22^{c}
9e	49.23 ± 0.31^{c}	48.08 ± 0.562^{b}	50.91 ± 0.24^{b}	53.95 ± 0.71^{b}
10b	56.86 ± 0.32^{a}	62.85 ± 0.38^{a}	61.25 ± 0.71^{a}	61.12 ± 0.85^{a}
10c	50.32 ± 0.31^{bc}	45.14 ± 0.73^{c}	47.92 ± 0.73^{c}	45.37 ± 0.16^{d}
Dox	48.09 ± 0.43^{c}	44.67 ± 0.35^{c}	42.94 ± 0.27^{d}	44.08 ± 0.79^{d}

All values are expressed as mean ± SEM.
Different letters are significantly different in the same column at $P < 0.05$.

ΔG = Gibb's free energy
NHA = non-hydrogen atom.
pIC_{50} = half-maximal inhibitory concentration (in molar concentration).

The lowest acceptable limit of LE is 0.3 [52].

The ligand efficiency concept has been recently extended to consider other physicochemical parameters, such as lipophilicity. Hence, the new metric "Liphophilic Ligand Efficiency" (LLE) was introduced. LLE is a measure of how efficiently a ligand can exploit its lipophilicity to bind to its target [53], thus highlighting the price paid in ligand lipophilicity on the expense of its potency. LLE can be calculated from the following equation:

$$LLE = pIC_{50} - cLogP$$

LLE values ≥ 3 are acceptable for lead compounds, while drug-like candidates record values ≥ 5 [50].

Herein, LE and LLE values of the most active compounds were calculated based on their IC_{50} values against the four screened cancer cell lines. Results (Table 7) indicated that compound **3a** had acceptable LE values (≥0.3) against all the screened cancer cell lines. Other compounds were slightly beyond the acceptable limit (0.238–0.281). Additionally, compound **3a** exhibited LLE values above the limit recommended for lead compound (> 3) against all the screened cancer cell lines, while other compounds showed LLE values in the range of 0.795–2.535.

3. Conclusion

This study portrays design and synthesis of novel pyridine and thienopyridine-based architectures as dual VEGFR-2/PIM-1 kinase inhibitors endowed with caspase 3/7 activation *via* merging their pharmacophoric features. All the newly synthesized compounds were screened for cytotoxicity against normal fibroblasts and four cancer cell lines (HepG-2, Caco-2, MCF-7 and PC-3) compared to doxorubicin utilizing MTT assay. The most active Compounds **3a, 9e, 10b** and **10c** exhibited higher anticancer potential than doxorubicin, against all the screened cell lines, especially HepG-2 with promising SI values. Their flow cytometric analysis data showed higher induced apoptosis-dependent death in the treated cancer cells compared to doxorubicin. Mechanistic studies revealed that they induced caspase 3/7 activation and DNA fragmentation higher than doxorubicin, with **10b** at the top of the list. VEGFR-2 inhibition assay showed that **10b** (IC_{50} = 5.873 µM) and **9e** (IC_{50} = 6.905 µM) exhibited comparable activities to quercetin (IC_{50} = 5.219 µM), whereas **10c** and **3a** were less active. PIM-1 kinase inhibitory assay revealed remarkable activities (IC_{50} = 7.948–12.163 µM) compared to quercetin (IC_{50} = 11.436 µM). Again, **10b** was the most potent (IC_{50} = 7.948 µM) among the group. Real time PCR assays showed that **3a, 9e, 10b** and **10c** exhibited higher therapeutic potential to alter the expression levels of VEGF, p53 and cyclin D than doxorubicin. Finally, their computational ligand efficiency metrics were reasonable. In light of these results, it could be concluded that the assembly of thienopyridine core, amide linker and terminal *p*-tolyl group **(10b)** conferred the highest dual VEGFR-2/PIM-1 kinase inhibition, best VEGF expression suppression and caspase 3/7 activation which were consistent with cytotoxicity results. Such architecture may pave the way for further optimization strategies towards new lead multitarget anticancer agents.

Table 5
In vitro VEGFR-2 and PIM-1 kinase inhibition data of the most active compounds.

Cpd No.	IC_{50} (µM)	
	VEGFR-2	PIM-1 kinase
3a	12.411	9.236
9e	6.905	9.394
10b	5.873	7.948
10c	9.188	12.163
Quercetin	5.219	11.436

Table 6
Change in the expression level of VEGF, p53 and Cyclin D in the most active compounds-treated HepG2.

Cpd No.	Fold change in gene expression level		
	VEGF	p53	Cyclin D
3a	0.26 ± 0.004^{b}	3.169 ± 0.001^{a}	0.187 ± 0.00003^{a}
9e	0.428 ± 0.007^{d}	2.359 ± 0.005^{b}	0.259 ± 0.006^{c}
10b	0.228 ± 0.006^{a}	3.1417 ± 0.006^{a}	0.175 ± 0.0001^{a}
10c	0.359 ± 0.007^{c}	2.24 ± 0.006^{d}	0.219 ± 0.0001^{b}
Dox	0.518 ± 0.01^{e}	1.9596 ± 0.02^{e}	0.304 ± 0.013^{d}

All values are expressed as mean ± SEM.
Different letters are significantly different in the same column at $P < 0.05$.

Table 4
Percentages of DNA fragmentation in the most active compounds-treated cancer cell lines.

Cpd No.	DNA fragmentation %			
	HepG-2	Caco-2	MCF-7	PC-3
Untreated Cells	1.69 ± 0.025^{d}	1.085 ± 0.055^{c}	2.03 ± 0.09^{d}	1.59 ± 0.02^{d}
3a	76.825 ± 1.18^{a}	50.675 ± 0.33^{b}	50.04 ± 0.17^{b}	59.234 ± 1.3^{b}
9e	61.925 ± 0.38^{b}	48.755 ± 1.11^{b}	59.31 ± 0.77^{b}	66.255 ± 1.28^{b}
10b	77.795 ± 1.25^{a}	79.892 ± 1.35^{a}	81.605 ± 0.93^{a}	90.24 ± 7.6^{a}
10c	65.39 ± 1.15^{b}	51.955 ± 0.71^{b}	51.845 ± 0.43^{b}	49.025 ± 0.08^{c}
Dox	42.825 ± 0.28^{c}	45.925 ± 0.28^{b}	42.005 ± 1.23^{c}	45.22 ± 0.35^{c}

All values are expressed as mean ± SEM.
Different letters are significantly different in the same column at $P < 0.05$.

Table 7
Ligand Efficiency (LE) and Ligand Lipophilic Efficiency (LLE) of the most active compounds.

Cpd No.	NHA[a]	LogP[b]	HepG-2			Caco-2			MCF-7			PC-3		
			pIC_{50}[c]	LE	LLE	pIC_{50}	LE	LLE	pIC_{50}	LE	LLE	pIC_{50}	LE	LLE
3a	35	4.49	7.910	0.309	3.42	7.987	0.312	3.497	7.744	0.303	3.254	7.679	0.300	3.189
9e	39	6.83	7.886	0.277	1.056	7.625	0.267	0.795	7.787	0.273	0.957	7.793	0.273	0.963
10b	40	5.90	8.207	0.281	2.307	7.686	0.263	1.786	6.988	0.239	1.088	6.978	0.238	1.078
10c	41	5.51	8.045	0.268	2.535	7.621	0.254	2.111	7.772	0.259	2.262	7.694	0.257	2.184

[a] NHA: non-hydrogen atom.
[b] LogP: logarithm of compound partition coefficient between *n*-octanol and water.
[c] $pIC_{50} = -\log(IC_{50})$.

4. Experimental

4.1. Chemistry

All chemicals and solvents were purchased from commercial suppliers. Melting points were determined in open-glass capillaries using a Griffin melting point apparatus and were uncorrected. The progress of the reactions was monitored by thin-layer chromatography (TLC) on commercially available precoated silica gel aluminum-backed plates and the spots were visualized by exposure to iodine vapors or UV-lamp at λ 254 nm for few seconds. Infrared spectra (IR) were recorded, for KBr discs, on a PerkinElmer RXIFT-IR. Nuclear magnetic resonance spectra, ^{1}H NMR spectra were recorded on Bruker spectrometer (400 MHz) using DMSO-d_6 as solvent. The data were reported as chemical shifts or δ values (ppm) relative to tetramethylsilane (TMS) as internal standard. Signals were indicated by the following abbreviations: s = singlet, d = doublet, t = triplet, q = quartet and m = multiplet, dd = doublet of doublet and br. = broad. ^{13}C NMR pectra were detected on Bruker spectrometer (100 MHz) using DMSO-d_6 as solvent. The data were reported as chemical shifts or δ values (ppm) relative to tetramethylsilane (TMS) as internal standard. Microanalyses were within ± 0.4% of the calculated values.

4.1.1. 4,6-bis(3,4-Dimethoxyphenyl)-2-thioxo-1,2-dihydropyridine-3-carbonitrile (1)

A mixture of 3,4-dimethoxybenzaldehyde (1.66 g, 0.01 mol), 3,4-dimethoxyacetophenone (1.8 g, 0.01 mol), cyanothioacetamide (1.13 g, 0.01 mol) and anhydrous ammonium acetate (7.71 g, 0.1 mol) in ethanol (50 ml) was stirred and heated under reflux for 12 h. The reaction mixture was allowed to cool and the obtained precipitate was filtered, washed with cold ethanol, dried and crystallized from DMF/ethanol (2:1). Yield: 49%; MP: 222–4 °C; IR (KBr, cm^{-1}): 3444 (NH), 2216 (CN), 1518 (C═C), 1596, 1387, 1251, 1151 (*N*-C═S). ^{1}H NMR (DMSO-d_6, 400 MHz) δ ppm: 3.88 (s, 12H, 4 OCH_3), 7.09–7.17 (m, 3H, 3,4-dimethoxyphenyl-$C_{2,5\ \&\ 5'}$-H), 7.33–7.34 (m, 2H, 3,4-dimethoxyphenyl-$C_{6\ \&\ 2'}$-H), 7.51–7.55 (m, 2H, pyridyl-C_5-H & 3,4-dimethoxyphenyl-$C_{6'}$-H). Anal. Calcd (%) for $C_{22}H_{20}N_2O_4S$ (408.47): C, 64.69; H, 4.94; N, 6.86. Found: C, 64.67; H, 4.88; N, 6.76.

4.1.2. 4,6-bis(3,4-Dimethoxyphenyl)-2-(substitutedthio)nicotinonitrile (2a-d)

To a mixture of **1** (0.1 g, 0.25 mmol), anhydrous potassium carbonate (0.14 g, 1 mmol) in absolute ethanol (5 ml), the appropriate alkyl or aralkyl halides (1.1 mmol) were added. The mixture was heated under reflux for 8 h. The reaction mixture was then cooled and treated with ice-cold water. The precipitate formed was filtered and purified by washing with hot ethanol.

4.1.2.1. 4,6-bis(3,4-Dimethoxyphenyl)-2-(methylthio)nicotinonitrile (2a).

Yield: 95%; MP: 178–80 °C; IR (KBr, cm^{-1}): 2207 (C≡N), 1565(C═N), 1517 (C═C), 1259 (C−O−C), 1025 (C−S−C); ^{1}H NMR (DMSO-d_6, 400 MHz, δ ppm): 2.74 (s, 3H, SCH_3), 3.86, 3.87 (2 s, each 6H, 4 OCH_3), 7.09,7.14 (2d, J = 8 *Hz*, each 1H, 3,4-dimethoxyphenyl-$C_{5\ \&\ 5'}$-H), 7.30 (d, J = 8 *Hz*, 1H, 3,4-dimethoxyphenyl-C_6-H), 7.34 (s, 1H, 3,4-dimethoxyphenyl-C_2-H), 7.85–7.87 (m, 2H, pyridyl-C_5-H & 3,4-dimethoxyphenyl-$C_{2'}$-H), 7.90 (d, J = 8 Hz, 1H, 3,4-dimethoxyphenyl-$C_{6'}$-H); ^{13}C NMR (DMSO-d_6, 100 MHz, δ ppm): 13.52, 56.05, 56.09, 56.14, 56.21, 102.08, 111.01, 112.18, 112.78, 115.23, 116.81, 121.35, 122.02, 128.50, 129.80, 149.17, 149.38, 150.83, 151.69, 154.12, 157.86, 163.37; Anal. Calcd for $C_{23}H_{22}N_2O_4S$ (422.50): C, 65.38; H, 5.25; N, 6.63. Found: C, 65.28; H, 5.19; N, 6.62.

4.1.2.2. 4,6-bis(3,4-Dimethoxyphenyl)-2-(ethylthio)nicotinonitrile (2b).

Yield: 91%; MP: 128 °C; IR (KBr, cm^{-1}):2214 (C≡N), 1567 (C═N), 1515 (C═C), 1266 (C−O−C), 1023 (C−S−C); ^{1}H NMR (DMSO-d_6, 400 MHz, δ ppm): 1.45 (t, J = 8 *Hz*, 3H, $SCH_2\underline{CH_3}$), 3.39 (q, J = 8 *Hz*, 2H, $S\underline{CH_2}CH_3$), 3.86–3.88 (m, 12H, 4 OCH_3), 7.12,7.16 (2d, J = 8 *Hz*, each 1H, 3,4-dimethoxyphenyl-$C_{5\ \&\ 5'}$-H), 7.31 (d, J = 8 *Hz*, 1H, 3,4-dimethoxyphenyl-C_6-H), 7.35 (s, 1H, 3,4-dimethoxyphenyl-C_2-H), 7.85–7.87 (m, 2H, pyridyl-C_5-H & 3,4-dimethoxyphenyl-$C_{2'}$-H), 7.90 (d, J = 8 Hz, 1H, 3,4-dimethoxyphenyl-$C_{6'}$-H); Anal. Calcd for $C_{24}H_{24}N_2O_4S$ (436.52): C, 66.03; H, 5.54; N, 6.42. Found: C, 65.98; H, 5.51; N, 6.39.

4.1.2.3. 4,6-bis(3,4-Dimethoxyphenyl)-2-(propylthio)nicotinonitrile (2c).

Yield: 89%; MP: 138–40 °C; IR (KBr, cm^{-1}): 2213 (C≡N), 1566(C═N), 1518 (C═C), 1256 (C−O−C), 1021 (C−S−C); ^{1}H NMR (DMSO-d_6, 400 MHz, δ ppm): 1.06 (t, J = 8 *Hz*, 3H, $SCH_2CH_2\underline{CH_3}$), 1.77–1.86 (m, 2H, $SCH_2\underline{CH_2}CH_3$), 3.35–3.38 (m, 2H, $S\underline{CH_2}CH_2CH_3$), 3.86–3.88 (m, 12H, 4 OCH_3), 7.12,7.15 (2d, J = 8 *Hz*, each 1H, 3,4-dimethoxyphenyl-$C_{5\ \&\ 5'}$-H), 7.31 (d, J = 8 *Hz*, 1H, 3,4-dimethoxyphenyl-C_6-H), 7.35 (s, 1H, 3,4-dimethoxyphenyl-C_2-H), 7.83–7.86 (m, 2H, pyridyl-C_5-H & 3,4-dimethoxyphenyl-$C_{2'}$-H), 7.89 (d, J = 8 Hz, 1H, 3,4-dimethoxyphenyl-$C_{6'}$-H); Anal. Calcd for $C_{25}H_{26}N_2O_4S$ (450.55): C, 66.64; H, 5.82; N, 6.22. Found: C, 66.63; H, 5.81; N, 6.20.

4.1.2.4. 2-(Benzylthio)-4,6-bis(3,4-dimethoxyphenyl)nicotinonitrile (2d).

Yield: 81%; MP: 130–1 °C; IR (KBr, cm^{-1}): 2212 (C≡N), 1567 (C═N), 1513 (C═C), 1264 (C−O−C), 1025 (C−S−C); ^{1}H NMR (DMSO-d_6, 400 MHz, δ ppm): 4.71 (s, 2H, SCH_2), 3.80 (s, 3H, OCH_3), 3.84–3.86 (m, 9H, 3 OCH_3), 7.08,7.13 (2d, J = 8 *Hz*, each 1H, 3,4-dimethoxyphenyl-$C_{5\ \&\ 5'}$-H), 7.26–7.35 (m, 5H, benzyl-H), 7.49–7.51 (m, 2H, 3,4-dimethoxyphenyl-$C_{2\ \&6}$-H), 7.81 (s, 1H, 3,4-dimethoxyphenyl-$C_{2'}$-H), 7.86 (s, 1H, pyridyl-C_5-H), 7.89 (d, J = 8 Hz, 1H, 3,4-dimethoxyphenyl-$C_{6'}$-H); ^{13}C NMR (DMSO-d_6, 100 MHz, δ ppm): 34.08, 56.01, 56.07, 56.11, 56.19, 101.97, 110.97, 112.10, 112.15, 112.79, 115.77, 116.70, 121.44, 122.03, 127.68, 128.45, 128.97, 129.16, 129.69, 138.08, 149.17, 149.41, 150.87, 151.73, 154.31, 157.97, 162.37; Anal. Calcd for $C_{29}H_{26}N_2O_4S$ (498.16): C, 69.86; H, 5.26; N, 5.62. Found: C, 69.79; H, 5.19; N, 5.56.

4.1.3. General procedure for preparation of compounds (3a,b)

To a mixture of **1** (0.1 g, 0.25 mmol), anhydrous potassium

carbonate (0.14 g, 1 mmol) in absolute ethanol (5 ml), ethyl bromoacetate or ethyl bromopropionate (1.1 mmol) was added. The mixture was heated under reflux for 8 h. The reaction mixture was then cooled and poured on ice-cold water. The precipitate formed was filtered and purified by washing with hot ethanol.

4.1.3.1. Ethyl 2-((3-cyano-4,6-bis(3,4-dimethoxyphenyl)pyridin-2-yl)thio) acetate (3a). Yield: 81%; MP: 162–3 °C; IR (KBr, cm^{-1}): 1742 (C═O),2206 (C≡N), 1567 (C═N), 1514 (C═C), 1265 (C—O—C), 1023 (C—S—C); ^{1}H NMR (DMSO-d_6, 400 MHz, δ ppm): 1.11 (t, *J* = 8 *Hz*, 3H, $CH_2\underline{CH_3}$), 3.86–3.87 (m, 9H, OCH_3), 3.91 (s, 3H, OCH_3), 4.09 (q, *J* = 8 *Hz*, 2H, $\underline{CH_2}CH_3$), 4.27 (s, 2H, SCH_2), 7.09,7.16 (2d, *J* = 8, 12 *Hz*, each 1H, 3,4-dimethoxyphenyl-$C_{5\ \&\ 5'}$-H), 7.33 (d, *J* = 8 *Hz*, 1H, 3,4-dimethoxyphenyl-C_6-H), 7.37 (s, 1H, 3,4-dimethoxyphenyl-*C*$_2$-H), 7.83 (s, 1H, pyridyl-C_5-H),7.86 (d, *J* = 8 *Hz,* 1H, 3,4-dimethoxyphenyl-$C_{6'}$-H), 7.90 (s, 1H, 3,4-dimethoxyphenyl-$C_{2'}$-H); ^{13}C NMR (DMSO-d_6, 100 MHz, δ ppm): 14.44, 32.96, 56.12, 56.17, 56.18, 56.22, 61.61, 101.80, 111.34, 112.02, 112.25, 112.81, 115.79, 116.61, 121.49, 122.04, 128.35, 129.51, 149.20, 149.41, 150.92, 151.82, 154.31, 158.11, 161.77, 169.13. Anal. Calcd for $C_{26}H_{26}N_2O_6S$ (494.56): C, 63.14; H, 5.30; N, 5.66. Found: C, 63.02; H, 5.34; N, 5.62.

4.1.3.2. Ethyl 3-((3-cyano-4,6-bis(3,4-dimethoxyphenyl)pyridin-2-yl)thio) propanoate (3b). Yield: 79%; MP: 268–70 °C; IR (KBr, cm^{-1}):2207 (C≡N), 1729 (C═O), 1550(C═N), 1507 (C═C), 1246 (C—O—C), 1019 (C—S—C); ^{1}H NMR (DMSO-d_6, 400 MHz, δ ppm): 1.19 (t, *J* = 8 *Hz*, 3H, $CH_2\underline{CH_3}$), 2.89, 3.61 (2 t, *J* = 8 *Hz*, each 1H, $SCH_2\underline{CH_2}$), 3.82–3.87 (m, 14H, SCH_2& 4OCH_3), 4.11 (q, *J* = 8 *Hz*, 2H, $\underline{CH_2}CH_3$), 7.01–7.18 (m, *4*H, 3,4-dimethoxyphenyl-$C_{2,5,6\&\ 5'}$-H), 7.35 (s, 1H, pyridyl-C_5-H), 7.65 (d, *J* = 12 *Hz,* 1H, 3,4-dimethoxyphenyl-$C_{6'}$-H), 7.90 (s, 1H, 3,4-dimethoxyphenyl-$C_{2'}$-H); ^{13}C NMR (DMSO-d_6, 100 MHz, δ ppm): 14.53, 25.66, 34.22, 55.99, 56.06, 56.16, 56.22, 60.75, 102.34, 110.87, 112.02, 112.65, 112.80, 115.79, 116.61, 121.31, 122.04, 128.46, 129.69, 148.75, 149.46, 150.87, 151.76, 154.47, 158.02, 162.30, 171.84; Anal. Calcd for $C_{27}H_{28}N_2O_6S$ (508.59): C, 63.76; H, 5.55; N, 5.51. Found: C, 63.78; H, 5.56; N, 5.49.

4.1.4. General procedure for preparation of compounds (4a-d), (5a-e) and 6

To a mixture of **1** (0.1 g, 0.25 mmol) and anhydrous sodium acetate (0.04 g, 0.5 mmol) in absolute ethanol (5 ml), either of the appropriate phenacyl bromide or the appropriate chloroacetanilide derivatives (1.1 mmol) was added and the reaction mixture was stirred for 10 h at room temperature. The reaction mixture was then poured onto ice cold water. The precipitated product was collected by filtration and purified by washing with cold ethanol.

4.1.4.1. 4,6-bis(3,4-Dimethoxyphenyl)-2-((2-oxo-2-phenylethyl)thio) nicotinonitrile (4a). Yield: 76%; MP: 188–90 °C; IR (KBr, cm^{-1}): 2209 (C≡N), 1702 (C═O), 1568 (C═N), 1513 (C═C), 1264 (C—O—C), 1023 (C—S—C); ^{1}H NMR (DMSO-d_6, 400 MHz, δ ppm): 3.42 (s, 3H, OCH_3), 3.78 (s, 3H, OCH_3), 3.86–3.87 (m, 6H, 2 OCH_3), 5.14 (s, 2H, SCH_2), 6.84, 7.17 (2d, *J* = 8 *Hz*, each 1H, 3,4-dimethoxyphenyl-$C_{5,\ 5'}$-H), 7.34 (d, *J* = 8 *Hz*, 1H, 3,4-dimethoxyphenyl-C_6-H), 7.37 (s, 1H, 3,4-dimethoxyphenyl-*C*$_2$-H),7.55–7.65 (m, *4*H, phenyl-$C_{3\ \&\ 5}$-H &3,4-dimethoxyphenyl- $C_{2'\&6'}$-H), 7.73 (t, *J* = 8 *Hz*, 1H, phenyl-C_4 -H), 7.84 (s, 1H, pyridyl-C_5-H), 8.13 (d, *J* = *8 Hz*, 2H, phenyl-$C_{2\ \&\ 6}$-H); Anal. Calcd for $C_{30}H_{26}N_2O_5S$ (526.16): C, 68.42; H, 4.98; N, 5.32. Found: C, 68.22; H, 4.77; N, 5.22.

4.1.4.2. 4,6-bis(3,4-Dimethoxyphenyl)-2-((2-oxo-2-(p-tolyl)ethyl)thio) nicotinonitrile (4b). Yield: 80%; MP: 180–2 °C; IR (KBr, cm^{-1}):2211 (C≡N), 1698 (C═O), 1594 (C═N), 1515 (C═C), 1264 (C—O—C), 1020 (C—S—C); ^{1}H NMR (DMSO-d_6, 400 MHz, δ ppm): 2.55 (s, 3H, CH_3), 3.54 (s, 3H, OCH_3), 3.77–3.99 (m, 9H, 3 OCH_3), 5.08 (s, 2H, SCH_2), 6.84, 7.12 (2d, *J* = 8 *Hz*, each 1H, 3,4-dimethoxyphenyl-$C_{5,\ 5'}$-H), 7.14–7.19 (m, 2H, 3,4-dimethoxyphenyl-$C_{2,6}$-H), 7.28–7.40 (m, 2H, 3,4-dimethoxyphenyl- $C_{2'\&6'}$-H), 7.49–7.65 (m,2H, p-chlorophenyl- $C_{3\ \&\ 5}$-H), 7.83 (s, 1H, pyridyl-C_5-H), 7.98–8.30 (d, *J* = *8 Hz*, 2H, p-chlorophenyl-$C_{2\ \&\ 6}$-H); ^{13}C NMR (DMSO-d_6, 100 MHz, δ ppm): 26.93, 38.41, 56.00, 56.22, 56.25, 57.22, 101.91, 111.50, 111.70, 112.05, 112.27, 112.66, 112.77, 117.88, 122.28, 122.48, 123.75,128.19, 129.54, 130.41, 133.38, 149.20, 149.25, 151.35, 152.20, 156.44, 158.10, 179.84, 190.99; Anal. Calcd for $C_{31}H_{28}N_2O_5S$ (540.63): C, 68.87; H, 5.22; N, 5.18. Found: C, 68.66; H, 5.21; N, 4.99.

4.1.4.3. 2-((2-(4-Chlorophenyl)-2-oxoethyl)thio)-4,6-bis(3,4-dimethoxyphenyl) nicotinonitrile (4c). Yield: 72%; MP: 164–5 °C; IR (KBr, cm^{-1}):2210 (C≡N), 1691 (C═O), 1571 (C═N), 1513 (C═C), 1263 (C—O—C), 1023 (C—S—C); ^{1}H NMR (DMSO-d_6, 400 MHz, δ ppm): 3.51 (s, 3H, OCH_3), 3.79 (s, 3H, OCH_3), 3.86–3.87 (m, 6H, 2 OCH_3), 5.09 (s, 2H, SCH_2), 6.82, 7.16 (2d, *J* = 8 *Hz*, each 1H, 3,4-dimethoxyphenyl-$C_{5,\ 5'}$-H), 7.33 (d, *J* = 8 *Hz*, 1H, 3,4-dimethoxyphenyl-C_6-H), 7.36 (s, 1H, 3,4-dimethoxyphenyl-*C*$_2$-H), 7.55–7.57 (m, *2*H, 3,4-dimethoxyphenyl- $C_{2'\&6'}$-H), 7.66 (d, *J* = *8 Hz*, 2H, p-chlorophenyl- $C_{3\ \&\ 5}$-H), 7.82 (s, 1H, pyridyl-C_5-H), 8.12 (d, *J* = *8 Hz*, 2H, p-chlorophenyl-$C_{2\ \&\ 6}$-H); ^{13}C NMR (DMSO-d_6, 100 MHz, δ ppm): 38.41, 55.60, 56.00, 56.17, 56.22, 101.91, 110.88, 111.69, 112.26, 112.80, 115.87, 116.73, 121.40, 122.03, 128.38, 129.45, 129.48, 130.77, 134.99, 139.11, 149.20, 149.22, 150.90, 151.75, 154.21, 158.08, 161.82, 192.42; Anal. Calcd for $C_{30}H_{25}ClN_2O_5S$ (561.05): C, 64.22; H, 4.49; N, 4.99. Found: C, 64.01; H, 4.39; N, 4.89.

4.1.4.4. 2-((2-(4-Bromophenyl)-2-oxoethyl)thio)-4,6-bis(3,4-dimethoxyphenyl) nicotinonitrile (4d). Yield: 70%; MP: 186–8 °C; IR (KBr, cm^{-1}):2210 (C≡N), 1693 (C═O), 1573 (C═N), 1513 (C═C), 1262 (C—O—C), 1024 (C—S—C); ^{1}H NMR (DMSO-d_6, 400 MHz, δ ppm): 3.51 (s, 3H, OCH_3), 3.80 (s, 3H, OCH_3), 3.86–3.87 (m, 6H, 2 OCH_3), 5.09 (s, 2H, SCH_2), 6.81, 7.17 (2d, *J* = 8 *Hz*, each 1H, 3,4-dimethoxyphenyl-$C_{5,\ 5'}$-H), 7.33 (d, *J* = 8 *Hz*, 1H, 3,4-dimethoxyphenyl-C_6-H), 7.36 (s, 1H, 3,4-dimethoxyphenyl-*C*$_2$-H), 7.54–7.56 (m, *2*H, 3,4-dimethoxyphenyl- $C_{2'\&6'}$-H), 7.80–7.83 (m,3H, p-bromophenyl- $C_{3\ \&\ 5}$-H & pyridyl-C_5-H), 8.05 (d, *J* = *8 Hz*, 2H, p-bromophenyl-$C_{2\ \&\ 6}$-H); Anal. Calcd for $C_{30}H_{25}BrN_2O_5S$ (605.50): C, 59.51; H, 4.16; N, 4.63. Found: C, 59.45; H, 3.98; N, 4.58.

4.1.4.5. 2-((3-Cyano-4,6-bis(3,4-dimethoxyphenyl)pyridin-2-yl)thio)-N-phenylacetamide (5a). Yield: 75%; MP: 206–8 °C; IR (KBr, cm^{-1}): 3267 (NH), 2215 (C≡N), 1667 (C═O), 1598 (C═N), 1517 (C═C), 1258 (C—O—C), 1023 (C—S—C); ^{1}H NMR (DMSO-d_6, 400 MHz, δ ppm): 3.76–3.89 (m, 12H, 4 OCH_3), 4.26, 4.34 (2 s, each 1H, SCH_2), 6.82–7.19 (m, 4H, 3,4-dimethoxyphenyl-$C_{2,5,\ 6\ \&5'}$-H), 7.30–7.36 (m, 3H, phenyl-$C_{3,\ 4\&\ 5}$-H), 7.49–7.54 (m, 2H, 3,4-dimethoxyphenyl- $C_{2'\&6'}$-H), 7.60 (d, *J* = 8 *Hz*, 2H, phenyl-$C_{2,6}$-H), 7.87 (s, 1H, pyridyl-C_5-H), 10.36, 13.94 (2 s, 1H, NH D_2O exchangeable); Anal. Calcd for $C_{30}H_{27}N_3O_5S$ (541.62): C, 66.53; H, 5.02; N, 7.76. Found: C, 66.45; H, 4.97; N, 7.78.

4.1.4.6. 2-((3-Cyano-4,6-bis(3,4-dimethoxyphenyl)pyridin-2-yl)thio)-N-(p-tolyl)acetamide (5b). Yield: 72%; MP: 190–2 °C; IR (KBr, cm^{-1}): 3277 (NH), 2216 (C≡N), 1663 (C═O), 1597 (C═N), 1517 (C═C), 1255 (C—O—C), 1024 (C—S—C); ^{1}H NMR (DMSO-d_6, 400 MHz, δ ppm): 2.25 (s, 3H, CH_3), 3.77–3.89 (m, 12H, 4 OCH_3), 4.23, 4.31 (2 s, each 1H, SCH_2), 6.83–7.19 (m, 5H, 3,4-dimethoxyphenyl-$C_{2,5,\ 6,2'\&\ 5'}$-H), 7.32–7.36 (m, 2H, tolyl-$C_{3,\ 5}$-H), 7.48 (d, *J* = 8 *Hz*, 2H, tolyl-$C_{2,6}$ -H), 7.52 (d, *J* = 8 *Hz*, 1H, 3,4-dimethoxyphenyl- $C_{6'}$-H), 7.87 (s, 1H, pyridyl-C_5-H), 10.27, 13.93 (2 s, 1H, NH D_2O exchangeable); ^{13}C NMR (DMSO-d_6, 100 MHz, δ ppm): 20.93, 44.03, 56.02, 56.19, 56.21, 56.25, 101.91, 111.70, 112.06, 112.66, 115.91, 117.88, 119.60,119.83, 122.03, 123.74, 128.46, 129.60, 129.69, 133.31, 136.43, 137.06, 149.00, 151.35, 152.11, 152.19, 156.45, 158.32, 164.84, 166.01,179.84; Anal. Calcd for $C_{31}H_{29}N_3O_5S$ (555.64): C, 67.01; H,

5.26; N, 7.56. Found: C, 67.02; H, 5.11; N, 7.44.

4.1.4.7. 2-((3-Cyano-4,6-bis(3,4-dimethoxyphenyl)pyridin-2-yl)thio)-N-(4-methoxyphenyl) acetamide (5c). Yield: 77%; MP: 220 °C; IR (KBr, cm^{-1}): 3290 (NH), 2214 (C≡N), 1663 (C═O), 1598 (C═N), 1515 (C═C), 1252 (C−O−C), 1025 (C−S−C);^{1}H NMR (DMSO-d_6, 400 MHz, δ ppm): 3.72–3.89 (m, 15H, 5 OCH_3), 4.22, 4.30 (2 s, each 1H, SCH_2), 6.87–6.92 (m, 3H, p-methoxyphenyl-$C_{3,\ 5}$-H &3,4-dimethoxyphenyl-$C_{2'}$-H), 7.11–7.19 (m, 2H, 3,4-dimethoxyphenyl-$C_{5,\ 5'}$-H), 7.32–7.36 (m, 2H, 3,4-dimethoxyphenyl-$C_{6,\ 6'}$-H), 7.49–7.53 (m, 3H, p-methoxyphenyl- $C_{2,\ 6}$-H& 3,4-dimethoxyphenyl-$C_{2'}$-H), 7.88 (s, 1H, pyridyl-C_5-H), 10.21, 13.94 (2 s, 1H, NH D_2O exchangeable); ^{13}C NMR (DMSO-d_6, 100 MHz, δ ppm): 43.98, 55.65, 56.18, 56.22, 56.23, 56.25, 101.93, 111.71, 112.05, 112.66, 114.34, 114.44,121.14,121.41, 122.28, 123.75, 128.19, 128.46, 129.72, 132.03, 132.70, 149.05, 149.39, 151.65, 152.20, 154.28, 156.09, 158.30, 164.60, 165.75, 179.84; Anal. Calcd for $C_{31}H_{29}N_3O_6S$ (571.64): C, 65.13; H, 5.11; N, 7.35. Found: C, 65.16; H, 4.88; N, 7.22.

4.1.4.8. N-(4-Chlorophenyl)-2-((3-cyano-4,6-bis(3,4-dimethoxyphenyl) pyridin-2-yl)thio) Acetamide (5d). Yield: 76%; MP: 212–14 °C; IR (KBr, cm^{-1}):3264 (NH), 2214 (C≡N), 1668 (C═O), 1602(C═N), 1517 (C═C), 1255 (C−O−C), 1022 (C−S−C); ^{1}H NMR (DMSO-d_6, 400 MHz, δ ppm): 3.77–3.89 (m, 12H, 4 OCH_3), 4.26, 4.33 (2 s, each1H, SCH_2), 6.81–7.19 (m, 2H, 3,4-dimethoxyphenyl-$C_{2\&5}$-H), 7.32–7.36 (m, 2H, 3,4-dimethoxyphenyl-$C_{5'\&\ 6'}$-H), 7.40 (d, $J = 8\,Hz$, 2H,p-chlorophenyl-$C_{3\ \&5'}$-H), 7.49–7.54 (m, 1H, 3,4-dimethoxyphenyl-$C_{6'}$-H),7.62–7.64 (m, 3H, p-chlorophenyl-$C_{2\ \&6'}$-H&3,4-dimethoxyphenyl-$C_{2'}$-H),7.88 (s, 1H, pyridyl-C_5-H), 10.44, 13.94 (2 s, 1H, NH D_2O exchangeable); Anal. Calcd. for $C_{30}H_{26}ClN_3O_5S$ (576.06): C, 62.55; H, 4.55; N, 7.29. Found: C, 62.51; H, 4.51; N, 7.27.

4.1.4.9. N-(4-Bromophenyl)-2-((3-cyano-4,6-bis(3,4-dimethoxyphenyl) pyridin-2-yl)thio) Acetamide (5e). Yield: 66%; MP: 200–2 °C; IR (KBr, cm^{-1}):3259 (NH), 2213 (C≡N), 1662 (C═O), 1594(C═N), 1517 (C═C), 1257 (C−O−C), 1021 (C−S−C);^{1}H NMR (DMSO-d_6, 400 MHz, δ ppm): 3.77–3.89 (m, 12H, 4 OCH_3), 4.33 (s, 2H, SCH_2), 6.80–7.19 (m, 3H, 3,4-dimethoxyphenyl-$C_{2,5\ \&5'}$-H), 7.32–7.36 (m, 2H, 3,4-dimethoxyphenyl-$C_{6\&\ 6'}$-H), 7.48–7.52 (m, 2H, p-bromophenyl-$C_{3\ \&5'}$-H), 7.58 (d, $J = 8\,Hz$, 2H,p-bromophenyl-$C_{2\ \&6'}$-H), 7.69–7.5 (m, 1H, 3,4-dimethoxyphenyl-$C_{2'}$-H), 7.88 (s, 1H, pyridyl-C_5-H), 10.51, 13.94 (2 s, 1H, NH D_2O exchangeable); Anal. Calcd. for $C_{30}H_{26}BrN_3O_5S$ (620.51): C, 58.07; H, 4.22; N, 6.77. Found: C, 58.12; H, 4.12; N, 6.68.

4.1.5. 2-((3-Cyano-4,6-bis(3,4-dimethoxyphenyl)pyridin-2-yl)thio) acetamide (6)

Yield: 79%; MP: 232 °C; IR (KBr, cm^{-1}): 3467, 3335 (NH_2), 2197 (C≡N), 1632 (C═O), 1577(C═N), 1523 (C═C), 1259 (C−O−C), 1025 (C−S−C); ^{1}H NMR (DMSO-d_6, 400 MHz, δ ppm): 3.84–3.88 (m, 12H, 4 OCH_3), 4.43 (s, 2H, SCH_2), 5.76 (s, 2H, NH_2 D_2O exchangeable), 7.06–7.11 (m, 2H, 3,4-dimethoxyphenyl-$C_{5\&\ 5'}$-H), 7.17–7.20 (m, 2H, 3,4-dimethoxyphenyl-$C_{2\&\ 6}$-H), 7.79–7.85 (m, 3H, thienopyridinyl-C_5-H & 3,4-dimethoxyphenyl-$C_{2'\&6'}$-H); ^{13}C NMR (DMSO-d_6, 100 MHz, δ ppm): 56.06, 56.14, 56.25, 73, 110.66, 112.15, 112.26, 112.91, 116.11, 118.75, 119.04, 120.95, 121.61, 128.60, 130.06, 148.12, 149.22, 149.49, 150.07, 150.73, 151.27, 156.92, 161.38; Anal. Calcd for $C_{24}H_{23}N_3O_5S$ (422.50): C, 61.92; H, 4.98; N, 9.03. Found: C, 61.89; H, 4.97; N, 8.99.

4.1.6. General procedure for preparation of compounds 7 and 8

A suspension of **3a** or **6** (0.24 g, 0.5 mmol) in freshly prepared solution of sodium ethoxide (prepared from 0.06 g, 2.6 mmol sodium metal in 5 ml absolute ethanol) was heated under reflux for 6 h. The reaction mixture was then cooled to room temperature and treated with ice cold water. The precipitate formed was filtered, washed with ethanol, dried and crystallized from DMF/ ethanol.

4.1.6.1. Sodium 3-amino-4,6-bis(3,4-dimethoxyphenyl)thieno[2,3-b] pyridine-2-carboxylate (7). Yield: 51%; MP: 230–2 °C; IR (KBr, cm^{-1}): 3477, 3330 (NH_2), 1743 (C═O), 1585 (C═N), 1515 (C═C), 1260 (C−O−C), 1023 (C−S−C); ^{1}H NMR (DMSO-d_6, 400 MHz, δ ppm): 3.83 (s, 6H, 2 OCH_3), 3.86, 3.88 (2 s, each 3H, 2 OCH_3), 5.62 (s, 2H, NH_2 D_2O exchangeable), 7.05–7.14 (m, 4H, 3,4-dimethoxyphenyl-$C_{2,5,6\ \&\ 5'}$-H), 7.62 (s, 1H, thienopyridinyl-C_5-H), 7.75–7.76 (m, 2H, 3,4-dimethoxyphenyl-$C_{2'\&6'}$-H); ^{13}C NMR (DMSO-d_6, 100 MHz, δ ppm): 56.02, 56.09, 56.11, 110.46, 111.99, 112.17, 112.21, 113.12, 117.21, 120.13, 121.55, 122.86, 130.47, 131.50, 140.40, 146.51, 148.81, 149.40, 149.47, 150.37, 153.31, 160.15, 168.94; Anal. Calcd for $C_{24}H_{21}N_2NaO_6S$ (488.49): C, 59.01; H, 4.33; N, 5.73. Found: C, 59.11; H, 4.30; N, 5.72.

4.1.6.2. 3-Amino-4,6-bis(3,4-dimethoxyphenyl)thieno[2,3-b]pyridine-2-carboxamide (8). Yield: 54%; MP: 220–1 °C;IR (KBr, cm^{-1}): 3465–3339 (2 NH_2), 1647 (C═O), 1592(C═N), 1513 (C═C), 1255 (C−O−C), 1024 (C−S−C); ^{1}H NMR (DMSO-d_6, 400 MHz, δ ppm): 3.83–3.89 (m, 12H, 4 OCH_3), 6.04 (s, 2H, NH_2 D_2O exchangeable), 7.07–7.20 (m, 6H, NH_2 D_2O exchangeable, 3,4-dimethoxyphenyl-$C_{2,5,6\&\ 5'}$-H), 7.75–7.82 (m, 3H, thienopyridinyl-C_5-H &3,4-dimethoxyphenyl-$C_{2'\&6'}$-H); ^{13}C NMR (DMSO-d_6, 100 MHz, δ ppm): 56.06, 56.11, 56.14, 56.17, 97.95, 110.63, 112.19, 112.25, 112.88, 118.26, 120.62, 121.13, 121.54, 129.44, 130.69, 146.27, 147.83, 149.11, 149.46, 149.83, 150.92, 155.79, 167.44; Anal. Calcd for $C_{24}H_{23}N_3O_5S$ (465.52): C, 61.92; H, 4.98; N, 9.03. Found: C, 61.88; H, 4.87; N, 8.99.

4.1.7. General procedure for preparation of compounds (9a-d) and (10a-e)

To a mixture of **1** (0.1 g, 0.25 mmol), anhydrous potassium carbonate (0.14 g, 1 mmol) in absolute ethanol (5 ml), either of the appropriate phenacyl bromide or the appropriate chloroacetanilide derivatives (1.1 mmol) was added. The mixture was heated under reflux for 8 h. The reaction mixture was then cooled and poured on ice-cold water. The precipitate formed was filtered and purified by washing with hot ethanol.

4.1.7.1. (3-Amino-4,6-bis(3,4-dimethoxyphenyl)thieno[2,3-b]pyridin-2-yl)(phenyl) methanone (9a). Yield: 62%; MP: 200–2 °C; IR (KBr, cm^{-1}): 3458, 3300 (NH_2), 1720 (C═O), 1597 (C═N), 1511 (C═C), 1252 (C−O−C), 1024 (C−S−C); ^{1}H NMR (DMSO-d_6, 400 MHz, δ ppm): 3.84–3.88 (m, 12H, 4 OCH_3), 7.08–7.24 (m, 6H, NH_2 D_2O exchangeable, 3,4-dimethoxyphenyl-$C_{2,5,6\ \&\ 5'}$-H), 7.54–7.63 (m, 3H, thienopyridinyl-C_5-H & 3,4-dimethoxyphenyl-$C_{2'\&6'}$-H), 7.79–7.85 (m, 5H, phenyl-H); ^{13}C NMR (DMSO-d_6, 100 MHz, δ ppm): 56.07, 56.13, 56.23, 103.31, 110.71, 112.18, 112.54, 112.59, 118.51, 119.81, 121.00, 121.43, 127.80, 128.95, 130.25, 131.59, 141.38, 149.33, 149.42, 149.46, 150.10, 151.11, 151.31, 157.92, 162.74, 189.22; Anal. Calcd for $C_{30}H_{26}N_2O_5S$ (526.16): C, 68.42; H, 4.98; N, 5.32. Found: C, 68.33; H, 4.78; N, 5.29.

4.1.7.2. (3-Amino-4,6-bis(3,4-dimethoxyphenyl)thieno[2,3-b]pyridin-2-yl)(p-tolyl) methanone (9b). Yield: 60%; MP: 210–2 °C; IR (KBr, cm^{-1}): 3471, 3345 (NH_2), 1740(C═O), 1602(C═N), 1513 (C═C), 1251 (C−O−C), 1026 (C−S−C); ^{1}H NMR (DMSO-d_6, 400 MHz, δ ppm): 2.42 (s, 1H, CH_3), 3.84–3.90 (m, 12H, 4 OCH_3), 7.08–7.23 (m, 6H, NH_2 D_2O exchangeable, 3,4-dimethoxyphenyl-$C_{2,5,6\&\ 5'}$-H), 7.36, 7.72 (2d, $J = 8\,Hz$, each 2H, p-tolyl-$C_{3,4,5\ \&\ 6}$-H), 7.79–7.86 (m, 3H, thienopyridinyl-C_5-H & 3,4-dimethoxyphenyl-$C_{2'\&6'}$-H); Anal. Calcd for $C_{31}H_{28}N_2O_5S$ (540.17): C, 68.87; H, 5.22; N, 5.18. Found: C, 68.79; H, 5.02; N, 5.01.

4.1.7.3. (3-Amino-4,6-bis(3,4-dimethoxyphenyl)thieno[2,3-b]pyridin-2-yl)(4-methoxyphenyl)methanone (9c). Yield: 62%; MP: 190–1 °C; IR (KBr, cm^{-1}): 3469, 3296 (NH_2), 1732(C═O), 1592(C═N), 1513 (C═C), 1252 (C−O−C), 1025 (C−S−C); ^{1}H NMR (DMSO-d_6, 400 MHz, δ ppm): 3.73–3.96 (m, 15H, 5 OCH_3), 7.05–7.27 (m, 6H,

NH_2 D_2O exchangeable, 3,4-dimethoxyphenyl-$C_{2,5,6\&\ 5'}$-H), 7.80–7.88 (m, 3H, thienopyridinyl-C_5-H & 3,4-dimethoxyphenyl-$C_{2'\&6'}$-H); ^{13}C NMR (DMSO-d_6, 100 MHz, δ ppm): 55.90, 56.06, 56.12, 56.21, 103.23, 110.68, 112.17, 112.51, 114.21, 118.49, 119.91, 120.97, 121.44, 129.00, 130.12, 130.29, 133.74, 149.16, 149.38, 149.46, 150.07, 150.76, 151.26, 157.41, 162.07, 162.49, 188.24; Anal. Calcd for $C_{31}H_{28}N_2O_6S$ (556.63): C, 66.89; H, 5.07; N, 5.03; S, 5.76. Found: C, 66.86; H 5.00; N, 5.69.

4.1.7.4. (3-Amino-4,6-bis(3,4-dimethoxyphenyl)thieno[2,3-b]pyridin-2-yl)(4-chlorophenyl) methanone (9d). Yield: 59%; MP: 226–8 °C; IR (KBr, cm^{-1}): 3467, 3290 (NH_2), 1724 (C═O), 1590(C═N), 1513 (C═C), 1255 (C−O−C), 1023 (C−S−C); ^{1}H NMR (DMSO-d_6, 400 MHz, δ ppm): 3.84–3.88 (m, 12H, 4 OCH_3), 7.06–7.23 (m, 6H, NH_2 D_2O exchangeable, 3,4-dimethoxyphenyl-$C_{2,5,6\&\ 5'}$-H), 7.62 (d, J = 8 *Hz*, 2H, p-chlorophenyl-$C_{3\&5}$-H), 7.79–7.85 (m, 5H, p-chlorophenyl-$C_{2\&6}$-H, thienopyridinyl-C_5-H & 3,4-dimethoxyphenyl-$C_{2'\&6'}$-H); ^{13}C NMR (DMSO-d_6, 100 MHz, δ ppm): 56.09, 56.12, 56.22, 103.00, 110.69, 112.16, 112.54, 118.57, 119.71, 121.05, 121.42, 128.83, 129.08, 129.78, 130.18, 136.34, 139.95, 149.42, 149.45, 150.12, 151.34, 151.44, 157.75, 162.73, 187.74; Anal. Calcd for $C_{30}H_{25}ClN_2O_5S$ (561.05): C, 64.22; H, 4.49; N, 4.99. Found: C 64.18; H, 4.45; N, 4.96.

4.1.7.5. (3-Amino-4,6-bis(3,4-dimethoxyphenyl)thieno[2,3-b]pyridin-2-yl)(4-bromophenyl) methanone (9e). Yield: 63%; MP: 232–3 °C; IR (KBr, cm^{-1}): 3467, 3291 (NH_2), 1724 (C═O), 1587 (C═N), 1512 (C═C), 1253 (C−O−C), 1024 (C−S−C); ^{1}H NMR (DMSO-d_6, 400 MHz, δ ppm): 3.84–3.88 (m, 12H, 4 OCH_3), 7.07–7.23 (m, 6H, NH_2 D_2O exchangeable, 3,4-dimethoxyphenyl-$C_{2,5,6\&\ 5'}$-H), 7.73–7.84 (m, 7H, p-bromophenyl-$C_{2,3,5\&6}$-H, thienopyridinyl-C_5-H & 3,4-dimethoxyphenyl-$C_{2'\&6'}$-H); ^{13}C NMR (DMSO-d_6, 100 MHz, δ ppm): 56.06, 56.09, 56.13, 56.23, 102.97, 110.71, 112.15, 112.56, 118.58, 119.71, 121.05, 121.43, 125.23, 128.86, 129.95, 130.18, 132.01, 140.30, 149.39, 149.44, 150.12, 151.35, 151.47, 157.75, 162.73, 187.79; Anal. Calcd for $C_{30}H_{25}BrN_2O_5S$ (605.50): C, 59.51; H, 4.16; N, 4.63. Found: C, 59.48; H, 4.16; N, 4.62.

4.1.7.6. 3-Amino-4,6-bis(3,4-dimethoxyphenyl)-N-phenylthieno[2,3-b]pyridine-2-carboxamide (10a). Yield: 61%; MP: 170–2 °C; IR (KBr, cm^{-1}): 3473, 3353 (NH_2, NH), 1630(C═O), 1593 (C═N), 1530 (C═C), 1245 (C−O−C), 1024 (C−S−C); ^{1}H NMR (DMSO-d_6, 400 MHz, δ ppm): 3.85–3.89 (m, 12H, 4 OCH_3), 6.18 (s, 2H, NH_2 D_2O exchangeable), 7.07–7.13 (m, 5H, 3,4-dimethoxyphenyl-$C_{2,5,5'\&\ 6'}$-H& phenyl-C_4-H), 7.31–7.35 (m, 2H, phenyl-$C_{3\&5}$-H), 7.68 (d, J = 8 *Hz*, 2H, phenyl-$C_{2\&6}$-H), 7.78–7.84 (m, 3H, thienopyridinyl-C_5-H & 3,4-dimethoxyphenyl-$C_{2'\&6'}$-H), 9.47 (s, 1H, NH D_2O exchangeable); ^{13}C NMR (DMSO-d_6, 100 MHz, δ ppm): 56.09, 56.14, 56.18, 56.51, 97.51, 110.72, 112.19, 112.27, 112.83, 118.48, 120.75, 120.88, 121.54, 121.81, 124.02, 128.89, 129.30, 130.60, 139.29, 147.46, 147.99, 149.17, 149.46, 149.90, 151.02, 156.22, 160.41, 164.38; Anal. Calcd for $C_{30}H_{27}N_3O_5S$ (541.62): C, 66.53; H, 5.02; N, 7.76. Found: C, 66.49; H, 5.01; N, 7.68.

4.1.7.7. 3-Amino-4,6-bis(3,4-dimethoxyphenyl)-N-(p-tolyl)thieno[2,3-b]pyridine-2-carboxamide (10b). Yield: 64%; MP: 160°Cdecomp.; IR (KBr, cm^{-1}): 3482, 3362 (NH_2, NH), 1628 (C═O), 1593 (C═N), 1512 (C═C), 1234 (C−O−C), 1022 (C−S−C); ^{1}H NMR (DMSO-d_6, 400 MHz, δ ppm): 2.28 (s, 3H, CH_3), 3.84–3.89 (m, 12H, 4 OCH_3), 6.15 (s, 2H, NH_2 D_2O exchangeable), 7.08–7.19 (m, 6H, 3,4-dimethoxyphenyl-$C_{5,\ 5',\ 2\ \&\ 6'}$-H& p-tolyl-$C_{3\&5}$-H), 7.55 (d, J = 8 *Hz*, 2H, p-tolyl-$C_{2\&6}$-H), 7.78–7.85 (m, 3H, thienopyridinyl-C_5-H & 3,4-dimethoxyphenyl-$C_{2'\&6'}$-H), 9.39 (s, 1H, NH D_2O exchangeable); ^{13}C NMR (DMSO-d_6, 100 MHz, δ ppm): 20.95, 56.06, 56.10, 56.16, 56.18, 97.64, 110.73, 112.21, 112.28, 112.84, 118.47, 120.74, 120.92, 121.54, 121.87, 129.30, 130.61, 133.01, 136.70, 147.25, 147.96, 149.16, 149.46, 149.89, 151.01, 156.14, 160.37, 164.26; Anal. Calcd for $C_{31}H_{29}N_3O_5S$ (555.64): C, 67.01; H, 5.26; N, 7.56. Found: C, 67.00; H, 5.27; N, 7.54.

4.1.7.8. 3-Amino-4,6-bis(3,4-dimethoxyphenyl)-N-(4-methoxyphenyl) thieno[2,3-b]pyridine-2-carboxamide (10c). Yield: 59%; MP: 160–2 °C; IR (KBr, cm^{-1}): 3471, 3349 (NH_2, NH), 1631 (C═O), 1590 (C═N), 1511 (C═C), 1242 (C−O−C), 1024 (C−S−C); ^{1}H NMR (DMSO-d_6, 400 MHz, δ ppm): 3.75 (s, 3H, $C_6H_4OCH_3$), 3.84–3.89 (m, 12H, 4 OCH_3), 6.13 (s, 2H, NH_2 D_2O exchangeable), 6.91 (d, J = 8 *Hz*, 2H, p-methoxyphenyl-$C_{3\&5}$-H), 7.09–7.12 (m, 2H, 3,4-dimethoxyphenyl-$C_{2\&6}$-H), 7.17 (d, J = 8 *Hz*, 2H, 3,4-dimethoxyphenyl-$C_{5\&\ 5'}$-H), 7.55 (d, J = 8 *Hz*, 2H, p-methoxyphenyl-$C_{2\&6}$-H), 7.78–7.84 (m, 3H, thienopyridinyl-C_5-H & 3,4-dimethoxyphenyl-$C_{2'\&6'}$-H), 9.36 (s, 1H, NH D_2O exchangeable); ^{13}C NMR (DMSO-d_6, 100 MHz, δ ppm): 55.63, 56.06, 56.11, 56.16, 56.18, 110.71, 112.21, 112.26, 112.88, 114.01, 118.37, 120.69, 121.11, 121.55, 123.71, 129.43, 130.70, 147.80, 149.14, 149.47, 149.86, 150.95, 155.88, 160.33, 164.29; Anal. Calcd for $C_{31}H_{29}N_3O_6S$ (571.64): C, 65.13; H, 5.11; N, 7.35. Found: C, 65.10; H, 5.02; N 7.29.

4.1.7.9. 3-Amino-N-(4-chlorophenyl)-4,6-bis(3,4-dimethoxyphenyl)thieno[2,3-b]pyridine-2-carboxamide (10d). Yield: 60%; MP: 202–4 °C; IR (KBr, cm^{-1}): 3467, 3362 (NH_2, NH), 1636(C═O), 1587(C═N), 1513 (C═C), 1245 (C−O−C), 1021 (C−S−C); ^{1}H NMR (DMSO-d_6, 400 MHz, δ ppm): 3.84–3.89 (m, 12H, 4 OCH_3), 6.19 (s, 2H, NH_2 D_2O exchangeable), 7.08–7.13 (m, 2H, 3,4-dimethoxyphenyl-$C_{2\&\ 6'}$-H), 7.17 (d, J = 8 *Hz*, 2H, 3,4-dimethoxyphenyl-$C_{5\&\ 5'}$-H), 7.38 (d, J = 8 *Hz*, 2H, p-chlorophenyl-$C_{3\&5}$-H), 7.73 (d, J = 8 *Hz*, 2H, p-chlorophenyl-$C_{2\&6}$-H), 7.79–7.85 (m, 3H, thienopyridinyl-C_5-H & 3,4-dimethoxyphenyl-$C_{2'\&6'}$-H), 9.59 (s, 1H, NH D_2O exchangeable); ^{13}C NMR (DMSO-d_6, 100 MHz, δ ppm): 56.07, 56.11, 56.18, 56.50, 97.50, 110.71, 112.21, 112.31, 112.81, 118.47, 120.80, 120.93, 121.54, 121.87, 123.18, 127.50, 128.79, 129.23, 131.01, 147.78, 148.09, 149.18, 149.46, 149.92, 151.05, 156.35, 160.36, 164.26; Anal. Calcd for $C_{30}H_{26}ClN_3O_5S$ (576.06): C, 62.55; H, 4.55; N, 7.29. Found: C, 62.49; H, 4.52; N, 7.28.

4.1.7.10. 3-Amino-N-(4-bromophenyl)-4,6-bis(3,4-dimethoxyphenyl) thieno[2,3-b]pyridine-2-carboxamide (10e). Yield: 61%; MP: 220–2 °C; IR (KBr, cm^{-1}): 3468, 3344 (NH_2, NH), 1634(C═O), 1598(C═N), 1508 (C═C), 1245 (C−O−C), 1020 (C−S−C); ^{1}H NMR (DMSO-d_6, 400 MHz, δ ppm): 3.78–3.96 (m, 12H, 4 OCH_3), 6.20 (s, 2H, NH_2 D_2O exchangeable),7.08–7.13 (m, 2H, 3,4-dimethoxyphenyl-$C_{2\&\ 6'}$-H), 7.17 (d, J = 8 *Hz*, 2H, 3,4-dimethoxyphenyl-$C_{5\&\ 5'}$-H), 7.38 (d, J = 8 *Hz*, 2H, p-chlorophenyl-$C_{3\&5}$-H), 7.73 (d, J = 8 *Hz*, 2H, p-chlorophenyl-$C_{2\&6}$-H), 7.79–7.85 (m, 3H, thienopyridinyl-C_5-H & 3,4-dimethoxyphenyl-$C_{2'\&6'}$-H), 9.53 (s, 1H, NH D_2O exchangeable); Anal. Calcd for $C_{30}H_{26}BrN_3O_5S$ (620.51): C, 58.07; H, 4.22; N, 6.77. Found: C 58.02; H, 4.21; N, 6.67.

4.2. Biological evaluation

All chemicals, solvents, media and kits were purchased from commercial suppliers. The utilized protocols and equipments are described as following under each section. Biological evaluation procedures were performed in Medical Biotechnology Department, Genetic Engineering and Biotechnology Research Institute, City of Scientific Research and Technological Applications (SRTA-City), Egypt.

4.2.1. Cytotoxicity screening

Normal human lung fibroblast Wi-38 cell line was used to detect cytotoxicity of the tested compounds compared to currently used anticancer drug (doxorubicin). Wi-38 cell line was subcultured in DMEM medium-contained 10% fetal bovine serum (FBS), seeded as 5×10^3 cells per well in 96-well cell culture plate and incubated at 37 °C in 5% CO_2 incubator. After 24 h for cell attachment, serial concentrations of

these compounds and doxorubicin (Dox) were incubated with Wi-38 cells for 72 h. Cell viability was assayed by MTT method [32]. Twenty microliters of 5 mg/ml MTT (Sigma, USA) was added to each well and the plate was incubated at 37 °C for 3 h. Then MTT solution was removed, 100 µL DMSO was added and the absorbance of each well was measured with a microplate reader (BMG LabTech, Germany) at 570 nm. The effective concentration (IC_{50}) and safe dose (EC_{100}) values of the tested compounds that cause 50% and 100% cell viability were estimated by the GraphpadInstat software.

4.2.2. Anticancer screening

Anticancer effect of the above-mentioned compounds was assayed using four human cancer cell lines. Colon cancer cells (Caco-2) were maintained in DMEM (Lonza, USA) containing 10% FBS while breast cancer cell line (MCF-7), liver cancer cell line (HepG-2) and prostate cancer cell line (PC-3) were cultured in RPMI-1640 (Lonza, USA) supplemented with 10% FBS. All cancer cells ($5x10^3$ cells/well) were seeded in sterile 96-well plates. After 24 h, serial concentrations of the tested compounds and Dox were incubated with four cancer cell linesfor 72 h at 37 °C in 5% CO_2 incubator. MTT method was done as described above [32]. The half maximal inhibitory concentration (IC_{50}) values were calculated using the GraphpadInstat software. Furthermore, cellular morphological changes before and after treatment with the most effective and safest anticancer compounds were investigated using phase contrast inverted microscope with a digital camera (Olympus, Japan).

4.2.3. Flow cytometric analysis of apoptosis

The IC_{50} of the most effective compounds and Dox were incubated for 72 h with Caco-2, MCF-7, HepG-2 and PC-3 cell lines. After trypsinization, the untreated and treated cells were incubated with annexin V/PI for 15 min.Then cells were fixed and incubated with streptavidin-fluorescein (5 µg/ml) for 15 min. The apoptosis-dependent anticancer effect was determined by quantification of annexin-stained apoptotic cells using the FITC signaldetector (FL1) against the phycoerythrin emission signal detector (FL2) [42].

4.2.4. Caspase 3/7 activation assay

The percentage of caspase 3/7 activation was quantified using the Caspase-Glo 3/7 kit following the manufacturer's instructions. This kit used a luminogenic substrate that was cleaved by caspases resulting in the generation of the luminescent signal. This signal was measured by the fluorescence omega microplate reader (BMG LabTech, Germany) at 490 nm excitation and 520 nm emission.

4.2.5. Evaluation of cancer cell damage by propidium iodide-staining assay

Propidium iodide (PI) stain was used to detect the percentage of cell damage due to its ability to penetrate and stain the chromatin of dead cells only. The most active compounds were incubated with human cancer cell lines in CO_2 incubator. After 72 h, the untreated and treated cells were washed with phosphate buffered saline (PBS) and incubated with PI (10 µg/mL) for 15 min. Then PI was discard, 100 µL PBS was added and plates were read using fluorescence plate reader (BMG LabTech, Germany) at 520 nm emission and 490 nm excitation. The percentage of DNA damage = [(fluorescence intensity of treated cells-fluorescence intensity of untreated cells)/ fluorescence intensity of treated cells)] × 100.

4.2.6. VEGFR-2 kinase inhibitory activity

The most active compounds were evaluated for *in vitro* VEGFR-2 kinase inhibitory activity utilizing VEGFR2 (KDR) Kinase Assay Kit - BPS Bioscience Corporation catalog # 40325, following the manufacturer's instructions [45].

4.2.7. PIM-1 kinase inhibitory activity

The most active anticancer compounds were tested for their ability to *in vitro* inhibit PIM-1 kinase utilizing PIM-1 Kinase Assay Kit – Promega Corporation catalog # V4032, following the manufacturer's instructions [46].

4.2.8. Real time PCR assay for quantifying vascular endothelial growth factor (VEGF), p53 and cyclin D expression levels

Total RNAs of untreated and the most effective anticancer compounds-treated HepG2 cells were extracted using Gene JET RNA Purification Kit (Thermo Scientific, USA) then cDNA was prepared using cDNA Synthesis Kit (Thermo Scientific, USA). Real time PCR was performed using Real time PCR was performed using SYBR green qPCR kit (Thermo Fisher Scientific, USA) and specific primers. These primers (Forward/Reverse) were 5′-CTACCTCCACCATGCCAAGT-3′/5′-GCAGT AGCTGCGCTGATAGA-3′, 5′-TAACAGTTCCTGCATGGGCGGC-3′/5′-AG GACAGGCACAAACACGCACC-3′ and 5′-CCGTCCATGCGGAAGATC-3′/ 5′- GAAGACCTCCTCCTCGCACT-3′ for VEGF, p53 andcyclin D genes, respectively. The $2^{-\Delta\Delta CT}$ equation was used to estimate change in gene expressions before and after treatment of HepG2 cells.

4.2.9. Statistical analysis

Data were expressed as mean ± standard error of the mean (SEM). Statistical significance was estimated by the multiple comparisons Tukey post-hoc analysis of variance (ANOVA) using the SPSS16 program. The differences were considered statistically significant at $p < 0.05$.

References

[1] M. Gallorini, A. Cataldi, V. di Giacomo, BioDrugs 26 (6) (2012) 377–391.
[2] L.A. Torre, F. Bray, R.L. Siegel, J. Ferlay, J. Lortet-Tieulent, A. Jemal, CA-Cancer J Clin. 65 (2) (2012) 87–108.
[3] Cancer. http://www.who.int/news-room/fact-sheets/detail/cancer. (Accessed 13 January 2019).
[4] H.P. Koeffler, F. McCormick, C. Denny, West J. Med. 155 (5) (1991) 505–514.
[5] M. Rebucci, C. Michiels, Biochem. Pharmacol. 85 (9) (2013) 1219–1226.
[6] N.M. Elsayed, R.A. Serya, M.F. Tolba, M. Ahmed, K. Barakat, D.A.A. El Ella, K.A. Abouzid, Bioorg. Chem. 82 (2019) 340–359.
[7] K. Holmes, O.L. Roberts, A.M. Thomas, M.J. Cross, Cell Signal. 19 (10) (2007) 2003–2012.
[8] S. Tugues, S. Koch, L. Gualandi, X. Li, L. Claesson-Welsh, Mol. Aspects Med. 32 (2) (2011) 88–111.
[9] K.J. Gotink, H.M. Verheul, Angiogenesis 13 (1) (2010) 1–14.
[10] R. Roskoski Jr, Biochem Bioph Res Co. 356 (2) (2007) 323–328.
[11] S. Wilhelm, C. Carter, M. Lynch, T. Lowinger, J. Dumas, R.A. Smith, B. Schwartz, R. Simantov, S. Kelley, Nat. Rev. Drug Discov. 5 (10) (2006) 835–844.
[12] M. Gou, H. Si, Y. Zhang, N. Qian, Z. Wang, W. Shi, G. Dai, Sci. Rep. UK 8 (1) (2018) 4602.
[13] M. Gross-Goupil, L. Françlois, A. Quivy, A. Ravaud, Clin Med Insights, Oncol. 7 (2013) 269–277.
[14] N. Imai, M. Shikami, H. Miwa, K. Suganuma, A. Hiramatsu, M. Watarai, A. Satoh, M. Itoh, A. Imamura, H. Mihara, M. Nitta, Brit J Haematol. 135 (5) (2006) 673–682.
[15] T.T. Zhao, D. Trinh, C.L. Addison, J. Dimitroulakos, PloS one 5 (9) (2010) e12563.
[16] R.H. Wenger, D.P. Stiehl, G. Camenisch, Sci. STKE 306 (2005) re12.
[17] E.B. Rankin, A.J. Giaccia, Cell Death Differ. 15 (4) (2008) 678–685.
[18] J. Hartwich, W.S. Orr, C.Y. Ng, Y. Spence, C. Morton, A.M. Davidoff, J. Pediatr. Surg. 48 (1) (2013) 39–46.
[19] A.L. Casillas, R.K. Toth, A.G. Sainz, N. Singh, A.A. Desai, A.S. Kraft, N.A. Warfel, Clin. Cancer Res. 24 (1) (2018) 169–180.
[20] C. Hogan, C. Hutchison, L. Marcar, D. Milne, M. Saville, J. Goodlad, N. Kernohan, D. Meek, J. Biol. Chem. 283 (26) (2008) 18012–18023.
[21] R.R. John, N. Malathi, C. Ravindran, S. Anandan, Mini review: Multifaceted role played by cyclin D1 in tumor behaviour, Indian J. Dental Res. 28 (2) (2017) 187–192.
[22] Y. Cao, E. Guangqi, E. Wang, K. Pal, S.K. Dutta, D. Bar-Sagi, D. Mukhopadhyay, Cancer Res. 72 (16) (2012) 912–3918.
[23] X. Jiang, H.E. Kim, H. Shu, Y. Zhao, H. Zhang, J. Kofron, J. Donnelly, D. Burns, S.C. Ng, S. Rosenberg, X. Wang, Science 299 (5604) (2003) 223–226.
[24] I.T. Weber, B. Fang, J. Agniswamy, Mini-Rev, Med Chem. 8 (11) (2008) 1154–1162.
[25] A. Ghith, K.M. Youssef, N.S. Ismail, K.A. Abouzid, Bioorg. Chem. 83 (2019) 111–128.
[26] K.A. Abouzid, G.H. Al-Ansary, A.M. El-Naggar, Eur. J. Med. Chem. 134 (2017) 357–365.
[27] M.E. Abdelaziz, M.M. El-Miligy, S.M. Fahmy, M.A. Mahran, A.A. Hazzaa, Bioorg. Chem. 80 (2018) 674–692.
[28] S.X. Cai, B. Nguyen, S. Jia, J. Herich, J. Guastella, S. Reddy, B. Tseng, J. Drewe, S. Kasibhatla, J. Med. Chem. 46 (12) (2003) 2474–2481.
[29] M.H. Badr, S.A.F. Rostom, M.F. Radwan, Chem. Pharm. Bull. 65 (5) (2017)

442–454.
[30] A. Malki, M. Mohsen, H. Aziz, O. Rizk, O. Shaban, M. El-Sayed, Z. Sherif, H. Ashour, Molecules 21 (2) (2016) 230.
[31] W. Gu, Y. Dai, H. Qiang, W. Shi, C. Liao, F. Zhao, W. Huang, H. Qian, Bioorg. Chem. 72 (2017) 116–122.
[32] T. Mosmann, J. Immunol. Methods 65 (1–2) (1983) 55–63.
[33] E.S. Al-Abdullah, Molecules 16 (4) (2011) 3410–3419.
[34] A.G. Al-Sehemi, E.A. Bakhite, J. Chin. Chem. Soc.-Taip. 52 (5) (2005) 975–985.
[35] M. Teleb, O.H. Rizk, F. Zhang, F.R. Fronczek, G.W. Zamponi, H. Fahmy, Bioorg. Chem. 83 (2019) 354–366.
[36] R.C.F. Jones, Amides, in: A.R. Katritzky, R.J.K. Taylor (Eds.), Comprehensive Organic Functional Groups Transformation II, second ed., Elsevier Science, 2004, Vol. 5, pp. 75–274.
[37] V.P. Litvinov, V.V. Dotsenko, S.G. Krivokolysko, Adv. Heterocycl. Chem. 93 (2007) 117–178.
[38] N.A.M. Akhir, L.S. Chua, F.A.A. Majid, M.R. Sarmidi, Br. J. Med. Med. Res. 1 (4) (2011) 397–409.
[39] B. Ekwall, V. Silano, A. Paganuzzi-Stammati, F. Zucco, Toxicity tests with mammalian cell cultures, in: P. Bourdeau (Ed.), Short-term toxicity tests for non-genotoxic effects, Wiley, 1990, pp. 75–82.
[40] P. Prayong, S. Barusrux, N. Weerapreeyakul, Fitoterapia 79 (7–8) (2008) 598–601.
[41] M.M. Abu-Serie, F.H. El-Rashidy, Recent Pat Anti-canc. 12 (3) (2017) 260–271.
[42] C. Riccardi, I. Nicoletti, Nat. Protocols 1 (3) (2006) 1458–1461.
[43] D.R. McIlwain, T. Berger, T.W. Mak, CSH Perspect. Biol. 7 (4) (2015).
[44] M.S. Ayoup, Y. Wahby, H.A. Hamid, M. Teleb, M.M. Abu-Serie, A. Noby, Eur. J. Med. Chem. 168 (2019) 340–356.
[45] http://bpsbioscience.com/vegfr2-kdr-kinase-assay-kit-40325.
[46] https://www.promega.com/-/media/files/resources/protocols/kinase-enzyme appnotes/pim1-kinase-assay.pdf?la = en.
[47] J. Logan, K. Edwards, N. Saunders, Real-time PCR: current technology and applications, Caister Academic Press, 2009.
[48] C.H. Reynold, B.A. Tounge, S.D. Bembenek, J. Med. Chem. 51 (8) (2008) 2432–2438.
[49] P.R. Andrews, D.J. Craik, J.L. Martin, J. Med. Chem. 27 (12) (1984) 1648–1657.
[50] M. Orita, K. Ohno, M. Warizaya, Y. Amano, T. Niimi, Method Enzymol. 493 (2011) 383–419.
[51] H. Chen, O. Engkvist, T. Kogej, Compound properties and their influence on drug quality, in: C. Wermuth, D. Aldous, P. Raboisson, D. Rognan (Eds.), The Practice of Medicinal Chemistry, fourth ed., Academic Press, 2015, pp. 379–393.
[52] G.M. Keserü, G.M. Makara, Nat. Rev. Drug Discov. 8 (3) (2009) 203–212.
[53] I. Jabeen, K. Pleban, U. Rinner, P. Chiba, G.F. Ecker, J. Med. Chem. 55 (7) (2012) 3261–3273.